Self-assembled monolayers of thiols and dithiols on gold: new challenges for a well-known system

C. Vericat,[a] M. E. Vela,[a] G. Benitez,[a] P. Carro[b] and R. C. Salvarezza*[a]

Received 1st October 2009
First published as an Advance Article on the web 24th February 2010
DOI: 10.1039/b907301a

Self-assembled monolayers (SAMs) of alkanethiols and dialkanethiols on gold are key elements for building many systems and devices with applications in the wide field of nanotechnology. Despite the progress made in the knowledge of these fascinating two-dimensional molecular systems, there are still several "hot topics" that deserve special attention in order to understand and to control their physical and chemistry properties at the molecular level. This *critical review* focuses on some of these topics, including the nature of the molecule–gold interface, whose chemistry and structure remain elusive, the self-assembly process on planar and irregular surfaces, and on nanometre-sized objects, and the chemical reactivity and thermal stability of these systems in ambient and aqueous solutions, an issue which seriously limits their technological applications (375 references).

1. A brief introduction to self-assembled monolayers

The term "self-assembly" refers to the spontaneous formation of discrete nanometre-sized units from simpler subunits or building blocks.[1] During the self-assembly process, the constituent subunits (atoms, molecules, biomolecules, simple biological structures, *etc*), combine in such a way that they form a secondary, more complex structure with fewer degrees of freedom. While biological membranes, cellular structures and even viruses and cells can be regarded as highly sophisticated self-assembled systems,[2] the simplest examples are certainly the so-called self-assembled monolayers (SAMs).[3] These are, in a few words, arrangements of molecules (or atoms) adsorbed on solid surfaces in which intermolecular forces play a key role and which can be spontaneously formed from solution or from vapour phase.

Each of the molecules that constitute the building blocks of the system can be divided into three different parts: the headgroup (linking group), the backbone (main chain), and the specific terminal (active) group. The headgroup guides the self-assembly process on each type of substrate, linking the hydrocarbon chain (of variable length) to the metal surface through a strong bond. The interactions among backbone hydrocarbon chains (involving van der Waals and hydrophobic forces) ensure an efficient packing of the monolayer and contribute to stabilize the structures with increasing chain length. The terminal group confers specific properties to the

[a] *Instituto de Investigaciones Fisicoquímicas Teóricasy Aplicadas (INIFTA), Universidad Nacional de La Plata—CONICET, Sucursal 4 Casilla de Correo 16 (1900) La Plata Argentina. E-mail: robsalva@inifta.unlp.edu.ar; Fax: +54 2214254642; Tel: +54 2214254430; Web: http//nano.quimica.unlp.edu.ar*
[b] *Departamento de Química Física, Universidad de la Laguna, La Laguna, Tenerife, Spain*

C. Vericat

Carolina Vericat received her MS degree in Chemistry (1998) and her PhD (2003) from La Plata National University, Argentina. She was a postdoctoral researcher at Prof. Wieckowski's group at the Department of Chemistry, University of Illinois (UIUC), USA (2003–2004) and at Prof. Sanz's group, Department of Physical Chemistry, University of Barcelona, Spain (2005–2006). Since 2006 she has been a CONICET Researcher at the SPM and Surface Physical Chemistry Laboratory at INIFTA. Her primary research interests are the study of SAMs by STM/AFM and the functionalization of nanostructures.

M. E. Vela

María Elena Vela received her PhD in Chemistry from the La Plata National University, Argentina in 1984. She became a Research Scientist of INIFTA, Argentina, in 1986, Professor of the Chemistry Department of La Plata National University in 1992 and she joined the scientific staff of the Scanning Probe Microscopy Laboratory at INIFTA in 1994. Her research interests span the fields of interfacial chemistry, nanostructured materials and surfaces derivatization.

surface (hydrophilic, hydrophobic), and can also be used to anchor different molecules, biomolecules, or nanostructures by weak interactions or covalent bonds.[2,4]

The ease of preparation and the fact that it is possible to prepare SAMs with different terminal groups (an important issue for many applications) has converted them to the most important type of organic monolayer. Also, SAMs can be formed not only on planar surfaces, but on objects of all sizes and with a variety of shapes. Among SAMs, the most popular, because of their promising and current applications in several fields of nanotechnology, are those of thiols and dithiols (and other S headgroup compounds, like disulfides and sulfides) on different oxide-free metals and, to a lesser extent, on semiconductors. For the formation of SAMs on hydroxylated surfaces (SiO_2/Si, Al_2O_3/Al, TiO_2/Ti, mica, glass, *etc*), silanes (alkyltrichlorosilanes, alkylalcoxysilanes, alkylaminosilanes, *etc*)[5–10] or phosphonates[10–17] are preferred. Other systems of interest are fatty acids on metal oxides (Al_2O_3, AgO, *etc*), and hydrocarbons on Si.[10]

G. Benitez

Guillermo Benitez received his PhD (2001) from La Plata National University, Argentina, working on thin metal films on semiconductors, under the guidance of Dr José M. Heras. In 2002 he joined the SPM and Surface Physical Chemistry Laboratory, directed by Dr Salvarezza. Since 2006 he has been a Research Scientist of CONICET at the Research Institute of Theoretical and Applied Physical Chemistry (INIFTA) in La Plata. His field of research is the study of self assembled monolayers and nanostructured surfaces using electron spectroscopies.

SAMs can be regarded as the interface between "two worlds": metals, semiconductors, and inorganic compounds, on one hand, and organic and biological materials (simple organic compounds, polymers, complex biomolecules, and even cells) on the other. They thus represent an easy way to link materials with totally different physical and chemical properties. Moreover, the self-assembly process can involve different levels of construction, in a similar way to protein formation.[18–22] This is the reason why SAMs are so important in the so-called "bottom-up" methods widely used in nanotechnology.

The applications of SAMs in nanotechnology are many and involve very different areas of expertise. Among them are their use for stabilization and functionalization of nanosized objects (nanoparticles, nanorods and nanowires),[2,23,24] which in turn are found to have plenty of applications. Other important uses of SAMs are in the field of material protection, where they are used as ultrathin layers for corrosion prevention[25–27] and friction reduction,[28] and as anti-stiction coatings in MEMs fabrication.[29] In the area of device fabrication, SAMs are used as building blocks in sensors, biosensors, actuators,[30,31] and molecular motors.[32] They are also employed as active or passive elements in electronic devices, transistors and switches, and act as "nano alligator clips" in single molecule circuits.[33] In nano/microfabrication, molecules that can self-assemble are employed as inks in microcontact printing and dip pen lithography, as resists in photolithography and shave lithography, and as anti-adherent layers in nanomolding and nanoreplication.[3,34] Finally, in biology and medicine these molecules are used as building blocks for the design of biomolecule carriers, for biorecognition assays, as coatings for implants, and as surface agents for changing cell and bacterial adhesion to surfaces[35,36] among many others uses.[1–3,37,38] Some of these applications are schematically shown in Fig. 1.

In the particular case of thiol and dithiol SAMs on gold they are used in the field of device fabrication as inks or resists in

P. Carro

Pilar Carro received her PhD from La Laguna University (ULL), Tenerife, Spain, in 1986. She became Professor of Physical Chemistry in the Physical Chemistry Department in 1992. Her field of research is Computational Chemistry. She carries out her scientific research activity in the Nanoscopic Techniques, Surfaces and Molecular Electrochemistry group of the Physical Chemistry Department at ULL.

R. C. Salvarezza

Roberto C. Salvarezza received his PhD from the University of Buenos Aires, Argentina (1981). He became a research scientist of CONICET at the Research Institute of Theoretical and Applied Physical Chemistry (INIFTA) in La Plata (1982). After working at the Physics of Condensed Matter and Physical Chemistry Departments in the University Autónoma de Madrid (Spain), in 1992 he founded the Scanning Probe Microscopy Laboratory at INIFTA. He is author of over 250 manuscripts on Electrochemistry, Surface Physics, and Nanotechnology. Dr Salvarezza is currently a Principal Researcher of CONICET, Head of the SPM and Surface Physical Chemistry Laboratory and Director of INIFTA.

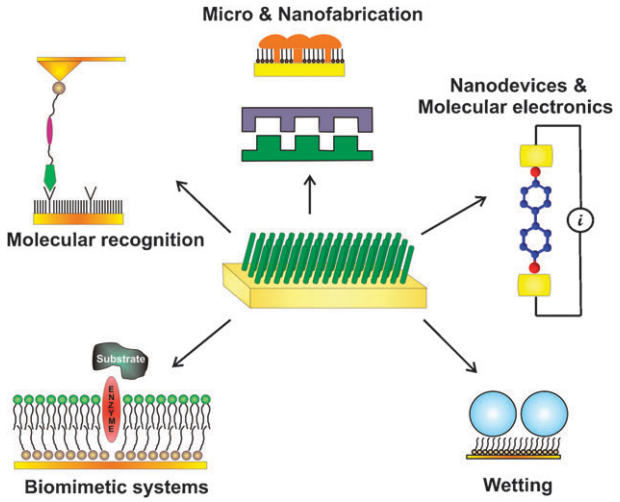

Fig. 1 Some applications of self-assembled monolayers in nanotechnology.

lithography for "writing" molecules and biomolecules on gold,[1–3,34] in molecular electronics (as passive or active parts in transistors and switches),[39–42] in sensors and biosensors (to immobilize different types of biomolecules, like DNA, enzymes, phospholipid membranes, bilayers and hybrid membranes, either on planar or irregular surfaces, or in nanoparticles and nanowires),[43–45] *etc*. Thiol SAMs are also important in the synthesis of gold nanoparticles, for stabilization of the nanostructures against aggregation[46] and to control the cluster size by tuning the hydrocarbon chain length.[47] In the field of biomedicine, thiol and dithiol SAMs are used as linkers or protective groups for biomolecule carriers (*e.g.*, for drug delivery purposes),[48] and also to functionalize the surface of medical devices such as gold stents.[37,49] Other applications of these SAMs include their use as chemical templates for crystallization of inorganic salts.[50,51]

Self-assembled monolayers have been studied by many different and complementary surface science techniques, both *in situ* (in the environment where the monolayers were formed) and *ex situ* (in a different environment, normally air). The reader can find a detailed discussion of these techniques in a previous review article.[52] Scanning probe microscopy techniques, mainly AFM and STM, are the most widely used characterization tools to determine the structural properties of SAMs, in particular, the arrangement of the molecules on the surface. These techniques (and many others which are derived from them) can be performed in ultra high vacuum (UHV), in liquids and in ambient conditions. Important advantages are the possibility to image non-periodic structures and SAM defects and to perform certain measurements in real time. Their main problem, however, is related to the local nature of the information they provide and to the need of image interpretation. Therefore, they should always be complemented with "average techniques", such as diffraction or spectroscopic studies.

Several diffraction techniques (electron, neutron, atom, ion, X-ray diffraction) have been employed to obtain information about the structure of the SAMs and the ordering of the chains and terminal groups. These techniques, which include XRD, GIXD, LEED and XPD (see Table 1 for definitions of acronyms), were the first to give structural information about ordered lattices in SAMs[53–60] and are still the best to obtain information on periodic structures. An important consideration when working with surface science techniques is that the molecules and bonds can be affected by electron irradiation, and, therefore, one has to be aware of the damage induced on the surface structure that could lead to misleading conclusions. Also, X-rays can have a damaging effect on the surface structure, which is not related to the X-rays themselves, but to the induced emission of secondary electrons.

In air and *in situ* vibrational spectroscopies, like IR, FTIR, IRRAS, SFG, HREELS, Raman spectroscopy, *etc*, have shed light on SAM packing density, crystalline order, molecular orientation, as well as the presence of some SAM defects.[61–66] HREELS also gives information about the adsorption sites of the molecules. Electron-based spectroscopies, such as AES, XPS and UPS, and X-ray absorption techniques with synchrotron radiation, like EXAFS and XANES, have played a major role in the study of the nature of the adsorbate–surface bond, the electronic properties of the adsorbed molecules, and are used to obtain information about chemical degradation of SAMs. Moreover, the above mentioned synchrotron techniques have been employed to study the structure and organization of the molecules on the substrates (packing density, crystalline order, molecular orientation, *etc*).[67–69] Ion-based spectroscopies, such as ISS and TOF-DRS, on the other hand, provide extremely accurate information about the outer functional groups,[70–73] while introducing little damage to the samples.

Other commonly used techniques include ellipsometry (to estimate the organic film thickness), TPD (for studying

Table 1 Acronyms of surface science techniques mentioned in the text

AES	Auger electron spectroscopy
AFM	Atomic force microscopy
CV	Cyclic voltammetry
DFT	Density functional theory
EIS	Electrochemical impedance spectroscopy
EXAFS	Extended X-ray absorption fine structure
GIXD	Grazing incidence X-ray diffraction
HREELS	High resolution electron energy loss spectroscopy
IR & FTIR	Infrared & Fourier transform infrared spectroscopy
IRRAS	Infrared reflection/absorption spectroscopy
ISS	Ion scattering spectroscopy
LEED	Low energy electron diffraction
MD	Molecular dynamics
NMR	Nuclear magnetic resonance
PMIRRAS	Polarization modulation infrared reflection/absorption spectroscopy
SFG	Sum frequency generation
STM	Scanning tunneling microscopy
TEM	Transmission electron microscopy
TOF-DRS	Time-of-flight direct recoil spectroscopy
TPD	Temperature programmed desorption
UPS	Ultraviolet photoelectron spectroscopy
XANES	X-ray absorption near edge structure
XPD	X-ray photoelectron diffraction
XPS	X-ray photoelectron spectroscopy
XRD	X-ray diffraction
XSW	X-ray standing waves

desorption kinetics), and electrochemical techniques (for stability studies in liquids and the study of SAM defects).

On the other hand, theoretical tools are of great importance in SAM studies. DFT calculations[74,75] can be regarded as the most extensive and successful approach for performing first-principle electronic structure and total energy calculations for a wide range of surfaces and materials, including adsorbed molecules on solid substrates. This theory uses the electron density function instead of the many-electron wavefunction to solve the Schrödinger equation. Usually, the term related to the exchange and electronic correlation is evaluated within the so called local density approximation (LDA), which is a very good approximation for strongly bound systems, but is inadequate for describing weaker bound structures (like van der Waals interactions). Thus, adsorption energies are usually overestimated, favouring more compact structures. A very different approach is the use of molecular dynamics (MD) simulations, which are based on molecular mechanics.[76] This method relies on the fact that a statistical ensemble average is considered equal to time averages of the system.

These methods are useful for verifying many aspects of the packing and phase behaviour of SAMs. In general, the combination of several local and average surface analysis techniques, together with theoretical techniques, has provided a thorough description of the SAM structures. However, as it will be seen later for the case of thiols and dithiols on gold, the existence of a huge amount of published papers in the field of SAMs from different groups describing measurements performed under very different conditions (both for experimental and theoretical techniques), has brought not little confusion to the SAM scientific community.

2. General aspects of thiol and dithiol SAMs on gold

Thiol and dithiol SAMs on metals, and particularly on Au, have attracted considerable attention due to their easy preparation from gas phase or from solution, and their relatively high stability mediated by the strength of the S–Au bond and by van der Waals interactions. These monolayers exhibit molecular order, and are relatively stable in ambient conditions. The most important SAMs (and by far, the most studied) are those of alkanethiols and, to a lesser extent, those of arenethiols, alkanedithiols and arenedithiols.[2]

Other SAMs on metals include those of dialkyldisulfides, and dialkylsulfides (see Fig. 2). It has also been reported that organic thiocyanates yield thiol SAMs on some metals.[77] All these molecules can be self-assembled on different metallic surfaces, like Au (the most important one and the aim of this review), but also Ag,[10,78–87] Cu,[70,88–90] Pd,[91–96] Pt,[95] Ni[97–103] and Fe.[104,105] In all cases oxide-free surfaces are needed to self-assemble the thiol monolayer. Thiol and other S-compound SAMs can also be formed on semiconductor surfaces, such as GaAs[106–108] and InP.[109,110] In this review we will only refer to thiol and dithiol SAMs on Au substrates.

A thiol molecule consists of three parts (Fig. 3): (1) the sulfur headgroup, which forms a strong, covalent bond with the substrate, (2) the hydrocarbon chain (of variable length), which stabilizes the SAM through van der Waals interactions,

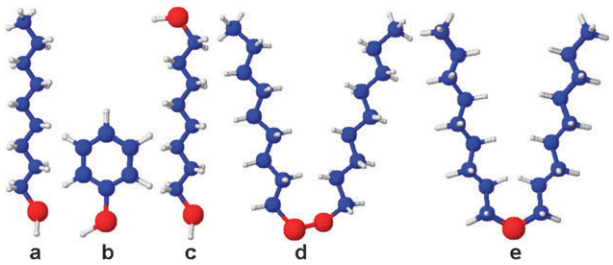

Fig. 2 Some examples of sulfur compounds that form self-assembled monolayers on metals and semiconductors: (a) alkanethiol (nonanethiol); (b) arenethiol (benzenethiol); (c) alkanedithiol (octanedithiol); (d) dialkyldisulfide (dinonyl disulfide); (e) dialkylsulfide (dinonyl sulfide). Red: S atom, blue: C atom, white: H atom.

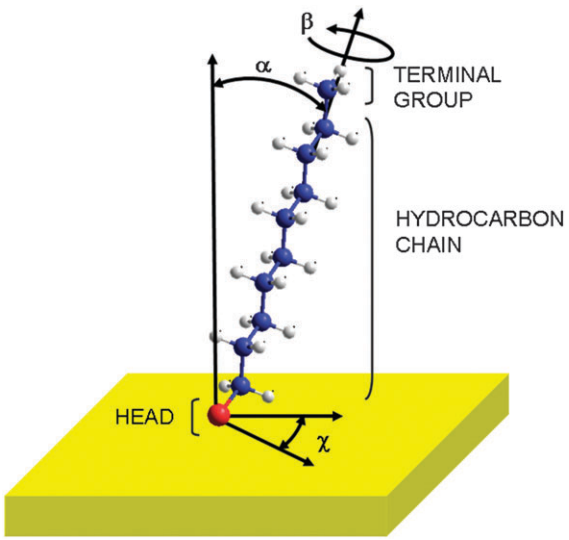

Fig. 3 Scheme of a decanethiol molecule adsorbed on Au(111) (yellow) in a standing up configuration. Typical angles are $\alpha = 30°$, $\beta = 55°$, and $\chi = 14°$. Red: sulfur atom; blue: carbon atom; white: hydrogen atom.

and (3) the terminal group, which can have different functionalities. A small change in the endgroup can be enough to change the physical and chemical properties of the layer.[3,111,112] Thus, $-CH_3$ and $-CF_3$ groups turn the SAM surface hydrophobic, metallophobic and highly anti-adherent,[113] while –COOH, $-NH_2$ or –OH groups yield hydrophilic surfaces with good metal ion and protein binding properties.[2,114] On the other hand, dithiols can be regarded as –SH-terminated thiols, and are very important to bind metallic ions and nanoparticles to the SAMs.[1,70]

The energy related to each part of the molecule has a different order of magnitude: 50 kcal mol^{-1} for the interaction between the S headgroup and the substrate (a thiolate bond); 1–2 kcal mol^{-1} per methylene for the van der Waals interactions between hydrocarbon chains; and only a few kT for energies related to the terminal groups.[115] However, all three parts of the molecule contribute to the structure and to the physical and chemical properties of the SAMs.

Since their discovery at the beginning of the 1980s by Nuzzo and Allara,[111] thiol and dithiol SAMs on gold have been

intensively studied with almost all existing surface science techniques. Thousands of papers and several reviews have been published which deal with different aspects of these SAMs, especially for gold planar surfaces (Au(111) is the model system), but also for curved surfaces and for nanoparticles. In these reviews the adsorption/desorption kinetics,[70,116] surface structures,[2,52,70,115,117,118] defects and dynamics,[2,52,118] charge transfer and electronic properties,[2,71,72] and also the applications of SAMs,[2,3] among others, have been extensively described.

However, more than 25 years later, many basic aspects of these SAMs remain controversial. In fact, still today, our knowledge about the chemistry of the alkanethiolate–Au bond in thiol SAMs on Au(111) is, at least, incomplete. Against the classical picture of a static, unreconstructed Au(111) surface with the molecules adsorbed at specific sites forming thiolate bonds, new experimental data and theoretical models have appeared in recent years.[119] These models propose a dynamical interaction between the adsorbates and the surface, which induces a strong reconstruction of the (111) surface involving the formation of thiolate–adatom moieties. Thiolate–Au complexes have been proposed as the building blocks of SAMs not only for planar surfaces, but also for the case of thiol-capped Au nanoparticles.[120] The knowledge of the S–Au interface structure and of the nature of the S–Au bond is relevant in molecular electronics and device fabrication, and also to understand the magnetic behaviour of thiol-capped gold nanoparticles.

Another issue that still needs to be elucidated deals with the structure of the adsorbate/substrate interface for the most important ordered lattices (both low- and high-coverage) as well as the origin of their contrast as imaged by STM.

The control of the quality of SAMs is also a key point in many technological problems. In the case of alkanethiols and dithiols SAMs there are many factors that affect their crystallinity. The "perfect" self-assembled monolayer is far from reality, and different types of defects exist which seriously limit their applications. An additional comment is required about the chemistry and structure of dithiol SAMs, which are difficult to control, since they depend more strongly on the self-assembly conditions than in the case of thiols.

As regards the stability against oxidation and thermal desorption of S headgroup compounds adsorbed on gold surfaces—either smooth, well-defined surfaces, or rough and disordered substrates (and even nanocurved surfaces, such as nanoparticles)—this is not just an academic problem, but also an important issue with practical implications. The search for strategies to increase the oxidation resistance of SAMs becomes crucial for their use in ambient conditions. The thermal fragility of SAMs, which are stable only up to 100 °C, is also a serious deficiency for practical applications. It is thus important to investigate the possibility of increasing stability against oxidation by a correct choice of the gold substrate.

It is the aim of this critical review to provide a thorough discussion of some of the "hot topics" above mentioned, together with some other related issues which are also of interest from the point of view of SAM applications.

3. The self-assembly process

Self-assembly has become one of the most useful strategy in bottom-up fabrication technologies, and the understanding of the fundamental mechanisms that drive this process, both from the kinetic and structural points of view, is relevant. The study of the driving forces involved during chemical self-assembly is imperative as scientists seek to build devices on the molecular scale. Therefore, an important amount of the work on self-assembling of organic monolayers on metal surfaces has focused on the adsorption kinetics of the alkanethiolate–gold system. Most of our knowledge about the self-assembly process on gold comes from studies on the Au(111) face, which is the model system for thiol and dithiol SAMs. In fact, still today there is only limited information about self-assembly of these molecules on other gold single crystal faces.[121–124]

Self assembly of thiols and dithiols on gold is, in principle, easy to perform and can be done both in the gas phase and in liquid environments (from solutions of different solvents), the latter being by far the most popular method because of its simplicity and accessibility in most laboratories.[2] In general, adsorption is performed in 10–1000 μM solutions of thiols, dithiols, dialkyldisulfides (in general S–S bonds break upon adsorption and thiolate SAMs are obtained) and dialkylsulfides in different solvents, depending on the nature of the molecule. Adsorption times also depend on the nature of the molecule: while 2–12 h are enough to form a well-ordered SAM in the case of long chain alkanethiols, at least 24 h are necessary for short chain alkanethiols or thiols with certain endgroups different from $-CH_3$.[71,72] For dithiol deposition from solution, shorter times have been reported.[125] On the other hand, methyldisulfide is the only possible reactant to prepare methylthiolate SAMs on Au(111), as the direct reaction of methylthiol with the Au(111) only results in physisorption of the molecules, *i.e.* there is no cleavage of the S–H bond.[126]

Thiols and dithiols adsorb on Au(111) to yield highly ordered arrays. STM, GIXD, LEED, atomic beam scattering, and TOF-DRS have indicated that SAM growth from the vapor is a complex process involving different steps.[127] It has been reported that during gas phase deposition the growth rate shows a complex dependence on pressure with different regimes: linear, quadratic, and saturated growth.[116] The simplest picture of this process (Fig. 4) implies an initial physisorption step, followed by chemisorption of the molecules, and finally the formation of crystalline, ordered domains with molecules in a closed-packed configuration.[127–130]

In UHV, the surface of the clean, adsorbate-free Au(111) substrate shows the well-known $22 \times \sqrt{3}$ Au(111) surface reconstruction (usually called herringbone reconstruction).[131] Upon thiol dosage there is an initial physisorption step, which is believed not to lift the reconstruction. Conversely to that observed for physisorbed alkanethiols on HOPG, where ordered arrays of lying down thiols are formed,[132] the physisorbed state on Au(111) can be described as a gas-like, highly disordered system (Fig. 4). The ability of alkanethiols to both physisorb through van der Waals interactions and to chemisorb through the sulfur headgroup provides an excellent

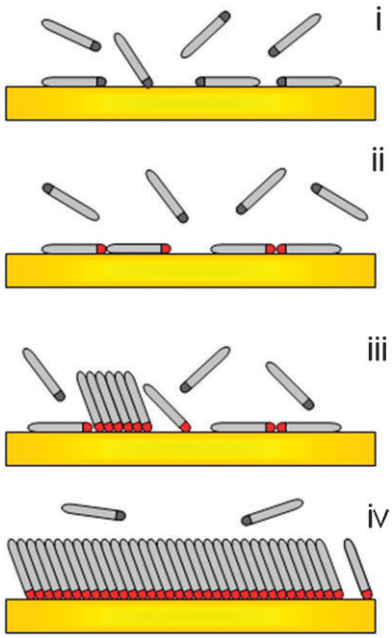

Fig. 4 Scheme of the different steps taking place during the self-assembly of alkanethiol on Au(111): (i) physisorption, (ii) lying down phase formation, (iii) nucleation of the standing up phase, (iv) completion of the standing up phase.

opportunity to study the role of the physisorbed precursor state in the chemisorption kinetics.

Although information about the physisorption step at the molecular level is difficult to obtain, as the mobile species cannot be observed by STM at room temperature, physisorbed methanethiol and dimethyl disulfide molecules have been imaged at 5 K.[133] Also, indirect evidence about this step has been reported for longer alkanethiolates.[134]

After physisorption, thiol molecules chemisorb on the Au(111) substrate through the S headgroup, forming a strong covalent bond, in a process that takes at least some minutes.[134] During the process the thiol molecule loses the mercaptan H atom, transforming itself in a thiolate. From the previous discussion we can write the adsorption process as follows

$$CH_3(CH_2)_nSH + Au \rightarrow (CH_3(CH_2)_nSH)_{phys}Au \quad (1a)$$

$$(CH_3(CH_2)_nSH)_{phys}Au \rightarrow CH_3(CH_2)_nS\text{–}Au + 1/2H_2 \quad (1b)$$

where reactions 1a and 1b correspond to thiol physisorption and chemisorption, respectively. The nature and mechanism of reaction (1b) is not completely understood. It has been proposed that this reaction occurs *via* oxidative adsorption of the alkanethiol RS–H bond to the metallic gold substrate,[115] although it is unknown whether the mechanism involves an ion, a radical, or another species. Concerning the nature of the S–Au bond, there is evidence from XPS, vibrational spectroscopy, mass spectrometry, and electrochemical techniques that thiols adsorb to form a strong covalent Au–S bond in which the chemical state of sulfur is similar to that found in thiolates.

On the other hand, there is still some controversy in the literature related to the S–H bond scission. In fact, there have been several studies that propose a non-dissociative adsorption for both short-chain alkanethiols on planar metal surfaces[135,136] and long-chain alkanethiols on gold clusters.[137] The exact fate of the thiol hydrogen atom upon adsorption also remains an issue of continued conjecture. The most accepted hypothesis is that the hydrogen atoms react to generate H_2, as shown in reaction 1b. Support for this reaction has been recently obtained from self-assembly results of nitroaromatic thiols on gold surfaces prepared by vacuum vapor deposition.[138] In that work a partial reduction of the terminal nitro groups (to yield amino groups) during SAM formation was found, which has been attributed to release of atomic hydrogen by the scission of S–H bonds during the formation of the thiolates.

Therefore, reaction (1b) seems to be valid for alkanethiol adsorption on Au(111) with the important exception of methanethiol on Au(111), where no dissociative S–H adsorption takes place. Indeed, experimental data from TPD, AES and low-temperature STM techniques found no evidence for S–H (or C–S) bond cleavage in adsorption of methanethiol on Au(111) at temperatures below 220 K.[136] This has been explained by the existence of an activation energy barrier of 0.3 eV, as already mentioned.

After discussing the reaction leading to chemisorption, we will focus on the growth process of the organic monolayer. It has been shown that chemisorption of the thiol molecules is easier at defective sites of the Au surface, *i.e.* steps edges, or at the "elbows" of the herringbone reconstruction, where preferred nucleation of islands containing lying down molecules (the so-called striped phases) takes place.[139] After nucleation, the islands grow, increasing the surface coverage of thiolate species on the Au surface. This growth is the origin of the initial rise in Fig. 5, where the H signal arising from the terminal methyl group detected by TOF-DRS is plotted against thiol exposure.[108] The completion of this lying down phase ($\sim 10^1$ L) is seen as a first plateau in Fig. 5. The presence of rotated domains in the STM images of the lying down phases is consistent with the nucleation and growth process.[129]

Increasing the exposure to $\sim 10^3$ L results in a sudden increase in the H signal, and this corresponds to the nucleation of molecules in the standing up configuration (Fig. 5). Then, the second plateau, which leads to saturation, corresponds to dense phases of upright molecules with a surface coverage $\theta \approx 1/3$. The completion of this process can take several hours,

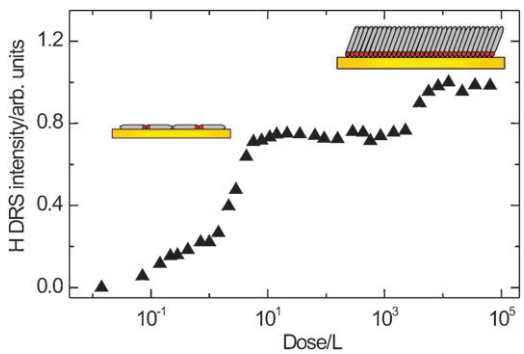

Fig. 5 Hydrogen DRS intensity from Au(111) *versus* exposure to hexanethiol in UHV. Data taken from ref. 108 with permission of the American Chemical Society. The schemes show the lying down and standing up phase formation corresponding to the two plateaus.

or even days, depending on the hydrocarbon chain length, and the result is the formation of ordered domains of molecules arranged in a closely packed, crystalline configuration.

The high coverage phases are an important part of this review and will be discussed in section 4.2. Also in this case the nucleation and growth of standing up islands in the lying down phase-covered Au(111) explains the presence of rotated domains, with clearly noticeable domain boundaries (see Fig. 13).

AFM and STM studies suggest that this picture and the reactions involved are also true for SAM growth from solution, irrespective of the solvent used.[128] However, in this case, the situation is more complex because it involves the displacement of the adsorbed solvent molecules so that the solvated thiol molecules can reach the adsorption site on the Au surface.[71,72] In general, it is very difficult to detect the lying down phase when the adsorption process is made from ethanolic or hexane solutions or from pure thiols because the system evolves rapidly to the standing up surface structure. The preparation of lying down structures from the liquid phase has been done by controlled desorption in UHV of denser phases formed in solution[140] or by controlled annealing in ethanol at 60 °C.[118]

On the other hand, the self-assembly process of dithiols is considered to take place following a pathway similar to that of monothiols.[141] In this case the reaction between the molecules and the gold surface can be expressed as

$$HS(CH_2)_nSH + Au \rightarrow (HS(CH_2)_nSH)_{phys}Au \quad (2a)$$

$$HS(CH_2)_nSH_{phys}Au + Au \rightarrow Au\text{–}S(CH_2)_nS\text{–}Au + H_2 \quad (2b)$$

However, in contrast to alkanethiols (reaction 1), reaction (2) leads to the formation of two thiolate bonds per molecule and, as it will be discussed later, these bonds can hinder to some extent the transition from the lying down to the standing up configuration, in particular for short dithiols, for which the gain in energy is smaller because of the smaller chain–chain interactions. The fact that it is possible to obtain a dithiol standing up phase from the lying down phase, both in solution and vapor phases, is surprising, since this process involves the rupture of the very stable gold–thiolate bonds. A possible explanation for the existence of the transition to the standing up phase could be a hydrogen exchange reaction between an incident free dithiol molecule (either in gas phase or in solution) and a chemisorbed lying down dithiolate on Au.[125] This reaction can be written as

$$Au\text{–}S(CH_2)_nS\text{–}Au + HS(CH_2)_nSH \rightarrow 2\,[Au\text{–}S(CH_2)_nSH] \quad (3)$$

This would result in the release of one of the ends of the chemisorbed molecule and in chemisorption of the free dithiol, thus leading to two standing up chemisorbed dithiols.

Moreover, it has also been observed that the lying down–standing up transition observed for thiol and dithiol adsorption on Au(111) is accompanied by a marked increase in surface stress. The origin of the surface stress, which will be discussed in more detail in section 6.2.2, seems to be related to changes in the electronic configuration of the substrate caused by the adsorption of thiol molecules.[142]

The self-assembly of thiols and dithiols involving lying down and standing up transitions is governed by the balance between intermolecular and molecule–substrate interactions and the gold surface response to the chemisorption process. The competing forces that determine the SAM ordered structure are the interaction between the headgroup and the substrate, which involves a large chemisorption energy, and the interchain van der Waals forces. Although van der Waals interactions are comparatively weak, they can have a significant influence on molecular self-assembly for the case of organic molecules with long hydrocarbon chains. The self-assembly takes place in two consecutive nucleation and growth processes that lead to rotated domains of lying down molecules, and later to domains of standing up molecules, irrespective of the environment used for SAM preparation. In the next section we will concentrate on the different lying down and standing up phases that give rise to the two plateaus observed in Fig. 5.

4. Ordered thiol and dithiol structures on Au(111)

In this section we will review the most important ordered surface structures found for thiol and dithiol SAMs on Au(111). The focus will be made on the aspects that have caused some controversy in the scientific community.

4.1 The striped phases

As mentioned before, the first step in the chemisorption process leads to the formation of domains of lying down molecules. In general, it is accepted that this process lifts the $22 \times \sqrt{3}$ surface reconstruction of the Au(111) surface leading to the (1×1) surface structure. However, in some studies, data have been shown that are consistent with direct chemisorption on the $22 \times \sqrt{3}$ reconstructed surface.[143]

Striped $p \times \sqrt{3}$ phases (p being an integer or half-integer) have been observed at early stages of growth from the vapour phase, both on non-reconstructed (1×1) and reconstructed $22 \times \sqrt{3}$ Au(111) surfaces, and also after controlled desorption of the dense phases produced from liquid adsorption (Fig. 6a).[129,143,144] For example, $23 \times \sqrt{3}$ and $11.5 \times \sqrt{3}$ surface structures have been reported for hexanethiol adsorption,[143] which have been assigned to lying down molecules in different arrangements. In some cases molecules adopt a S-head to S-head configuration and p is chain dependent, its value (multiplied by the Au–Au distance, 0.29 nm) corresponding to twice the one for the bulk molecule (Fig. 6b). In other cases, the molecules adopt S-head to hydrocarbon chain configuration, and p (times 0.29 nm) is also chain dependent but its value is in the order of the molecular size (Fig. 6c).[145] Striped phases have also been observed by STM for aromatic thiols.[146,147] In this case molecules are oriented with their axis parallel to the surface, in a similar way to what has been reported for alkanethiols on the same substrate.

The interpretation of the STM images obtained for this phase is still under debate. At first it was accepted that the bright spots indicated the position of the S headgroups. In fact, for the head-to-head configuration, it was proposed that they corresponded to adjacent S headgroups of the lying down

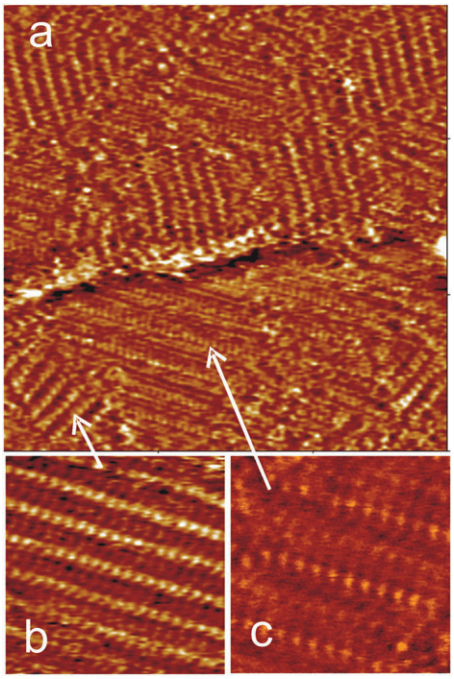

Fig. 6 STM images of two different striped phases for hexanethiol on Au(111). (a) 28.75 × 28.75 nm^2 image showing domains of the two different lying down phases (b) head-to-head configuration (8.75 × 8.75 nm^2 image); (c) head-to-tail configuration (6.75 × 6.75 nm^2 image).

molecules.[148] However, more recently, it has been proposed that the bright spots correspond to Au adatoms linked to two thiolate moieties.[133] The origin of these adatoms could be the lifting of the 22 × $\sqrt{3}$ Au(111) surface reconstruction that originates 1 adatom every 22 Au surface atoms.[133] The idea that thiolates form $(RS)_2Au$ complexes on the Au surface has been crucial for the present discussion of standing up phases and for a new overview of the chemistry of sulfur compounds on gold.[120] This has brought also a renewed interest in the general chemistry of gold, as we discuss in detail below.

As regards dithiols, striped phases are very important because the molecules form two thiolate bonds for each molecule. In some cases the interaction with the Au surface is so strong that these phases are not easily replaced by the standing up phases. Indeed, for the case of short alkanedithiols, it is expected that most of the monolayer will consist of molecules in the lying down configuration. This situation has been observed for butanedithiol and dithiothreitol (DTT), a related hydroxylated dithiol.[149] Even for the longer hexanedithiol (HDT), it has been reported that only ordered arrays of lying down molecules are formed both in gas phase and in liquid environment[150] In fact, it has been proposed that the striped phase acts as an efficient trap to hinder the lying down to standing up phase transition observed in Fig. 5, although mixed domains of standing up and lying down phases have been detected for HDT SAMs prepared in hexane solutions.[125] The behaviour of dithiol molecules on gold thus deserves particular attention because the surface structures seem to be strongly dependent on the length of the hydrocarbon chains.

4.2 The dense standing up phases

Due to the strong interaction between the alkanethiol S headgroup and the Au(111) substrate, the S headgroup chemisorbs on specific sites of the gold surface, forming lattices that are commensurate with the substrate. The order of the hydrocarbon chains has been studied by different IR spectroscopy techniques. From the analysis of CH_2 and CH_3 stretching modes it was found that at room temperature alkanethiols form a densely packed, crystalline-like assembly with fully extended alkyl chains in an all-*trans* configuration and with very few *gauche* defects. However, the degree of chain ordering is dependent on the chain length and substrate quality. This will be further addressed in Section 5.2.

Three angles fully define the orientation of the molecule in the standing up configuration with respect to the gold substrate: the tilt angle (α) is the angle between the molecular backbone and the surface normal direction; the twist angle (β) describes the rotation of the hydrocarbon chain plane with respect to the molecular axis; finally, the angle of precession (χ) gives the tilt direction and is derived from the projection of the inclination plane (defined by the substrate normal and the axis of the hydrocarbon chain) on the substrate plane.[70,151] This is schematically shown in Fig. 3. The α angle value is such as to allow the most effective close packing possible for the usually found S–S distances, thus maximizing van der Waals chain–chain interactions.[115] The tilt angle has been calculated from CH_2 and CH_3 group IR bands and ellipsometry data and turns out to be 30–35° for SAMs prepared from pure thiol or thiol ethanolic solutions.[135] In the next sections we will refer to the stable standing up lattices that are more commonly found. These are the $\sqrt{3} \times \sqrt{3}$ R30° lattice[152–157] and its related c(4 × 2) superlattices,[158,159] both found at saturation coverage. Other standing up phases have been observed before (or together with) the formation of the $\sqrt{3} \times \sqrt{3}$ R30° and c(4 × 2) surface structures, as we will briefly mention in section 4.3.

4.2.1 The $\sqrt{3} \times \sqrt{3}$ R30° lattice on Au(111). The $\sqrt{3} \times \sqrt{3}$ R30° alkanethiolate lattice exhibits a hexagonal symmetry with 0.5 nm distance between nearest neighbours. This is clearly seen in high resolution STM images (Fig. 7a), where the location of each molecule appears as a bright spot. This surface structure implies a surface coverage $\theta = 1/3$. However, also for this apparently simple lattice, the nature of the actual adsorption site and the related discussion about surface reconstruction and gold adatoms constitute by far the most controversial issue for thiol SAMs on Au(111) as will be discussed in detail in section 4.4.

It is well known that STM images provide valuable information on the local surface structure at the molecular level. However, since STM senses the local density of states (LDOS) near the Fermi level, it is not completely clear what the bright spots in Fig. 7a correspond to. In fact, they have been attributed to the terminal group of the hydrocarbon chain, the methylene units adjacent to the terminal group, or the S headgroups of the thiol molecules.[71,72,151,160,161] Some theoretical calculations made for STM imaging at high tunnelling resistance (low i_{tunnel}, high V_{bias}) favour the

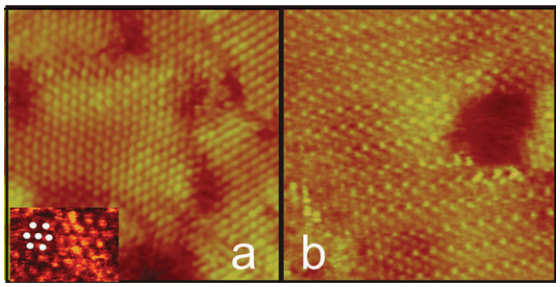

Fig. 7 13.5 × 13.5 nm^2 top view STM images of (a) a $\sqrt{3} \times \sqrt{3}$ R30° decanethiol lattice (the inset shows the same lattice on nonanedithiol). (b) a rectangular c(4 × 2) hexanethiol lattice. The bright spots indicate the position of the thiol molecules. The white dots in the inset indicate the hexagonal lattice.

hypothesis that the tip is actually probing the hydrocarbon chains or the terminal groups.[160–162] However, due to the wide variety of i_{tunnel} and V_{bias} conditions used in the different works, a generalization can be oversimplifying. The reader can find a detailed discussion about the dependence of the STM images on tunneling conditions for alkanethiolate SAMs on Au in the bibliography.[118,163] Due to the convolution between topographic and electronic effects the interpretation of STM images of alkanethiolate SAMs is always an important issue.

Similar images to those shown in Fig. 7a have been obtained for –COOH[164] and –NH_2[165] terminated thiols on Au(111), indicating that the $\sqrt{3} \times \sqrt{3}$ R30° lattice is a stable configuration that is not affected by the nature of the terminal groups.

In the case of dithiols, the dense phases of standing up molecules have been reported for molecules with hydrocarbon chains longer than $n = 6$.[150] For adsorption from the gas phase, short dithiols are usually handled because of their higher vapour pressures, and thus it is difficult to observe the lying down to standing up phase transition (very large dithiol doses are required). On the other hand, XPS and electrochemical data for dithiol SAMs grown in hexane solutions are consistent with the presence of a dense layer of molecules in the standing up configuration with $\theta \approx 1/3$.[144] For nonanedithiol SAMs prepared in toluene, $\sqrt{3} \times \sqrt{3}$ R30° domains were imaged by STM (inset in Fig. 7a), though in general these layers are not well organized and molecular resolution is difficult to attain.[149] Moreover, the fact that the metallic STM tip interacts very strongly with the –SH terminal group makes STM imaging with molecular resolution still more difficult.[125,149]

4.2.2 The c(4 × 2) superlattices. The existence of stable high coverage surface structures of thiolate on Au(111) other than the $\sqrt{3} \times \sqrt{3}$ R30° lattice was early detected by IR spectroscopy[166] and diffraction techniques:[159,158,165,166] there were peaks that could not be explained on the basis of a simple hexagonal lattice. These surface structures, which have the same coverage and tilt angle ($\alpha = 30°$) as the $\sqrt{3} \times \sqrt{3}$ R30°, were described as c(4 × 2) superlattices of the $\sqrt{3} \times \sqrt{3}$ R30° lattice, although it is more correct to describe them as (3 × 2$\sqrt{3}$)rect, taking into account the registry with the substrate. The c(4 × 2) superlattice unit cell is orthorhombic, and it is four times that of the $\sqrt{3} \times \sqrt{3}$ R30° lattice, which means that it contains four molecules. The c(4 × 2) structures had also been detected by STM in the early years of imaging.[167] Since then, different structures which can be described as c(4 × 2) have been imaged by many groups and in different environments, including UHV, air, and liquids with and without electrochemical control. Two of the more commonly found structures are the "zig–zag" and "rectangular" structures (the latter is shown in Fig. 7b), though many others have been found.[163,168]

In addition to thiols with methyl terminal groups, this structure has been imaged by STM for alkanethiols with other terminal groups like –COOH[164] –OH or –NH_2. This lattice has also been observed by STM for aromatic thiols, and in this case the molecular axis is orientated almost upright.[146] For dithiols some domains of the c(4 × 2) lattice embedded into disordered regions have been observed by STM for dithiothreitol on the Au(111) surface.[169]

The position of the alkanethiolate molecules on the substrate is highly speculative because, as in the case of the alkanethiolate $\sqrt{3} \times \sqrt{3}$ R30° lattice, it is not clear which type of gold sites are actually involved in the chemisorption. Thus, the elucidation of the real structure of the c(4 × 2) lattice has been (and still is) a matter of strong debate among experimental and theoretical surface scientists, and several models have been proposed to try to explain it.

Until recently, all proposed models made the assumption that the molecules were adsorbed on an unreconstructed (1 × 1) Au(111) surface. Since, for sterical reasons, α and χ can only have a single value for domains of closely packed alkanethiolate lattices (see Fig. 3), one of the early models proposed that the origin of the c(4 × 2) superlattices would be rows of molecules with two different β values. This model has been employed to explain STM contrast.[160] However, it was argued that differences in β would not be enough to explain diffraction data, and that there should be a displacement of the S headgroups with respect to the $\sqrt{3} \times \sqrt{3}$ R30° lattice.[158,170] The problem then was to determine the magnitude of this displacement.[171]

In this direction, an alternative model based on GIXD measurements[53] proposed that alkanethiolate molecules would adsorb forming disulfides with S–S distances of 0.22 nm with one of the S atoms in an fcc hollow and the other one in a bridge site. To achieve this, molecules would present *gauche* defects in the S–C bond, so that the hydrocarbon chains could have a hexagonal closed packing. Many efforts were unsuccessfully made to confirm this model, which was then discarded in the light of the results from other surface science techniques and a new interpretation of the GIXD data. A different model was proposed on the basis of the careful analysis of the distances between bright spots in STM images.[172] Measurements yielded some distances of 0.45 nm instead of 0.5 nm, and therefore, it was proposed that the molecules of the darker rows were in one type of site (*e.g.*, hollow site), and those in the brighter rows in another type of site (*e.g.*, bridge). An additional contribution from the presence of molecules with different β was compatible with the model. Still another model was proposed on the basis of GIXD data, in which S atoms were located in adjacent fcc and hcp hollow sites, with no evidence of pairing or dimer

formation.[173] A small substrate reconstruction that played an important role for the c(4 × 2) structure was proposed in that work.

Whatever the actual position of the molecules is, another interesting controversy that has arisen among scanning tunneling microscopists is related to the origin of the multiple structures imaged by STM. Indeed, it is not clear if they are due to a tip effect, an electronic effect due to changes in STM conditions (V_{bias}, $I_{setpoint}$ and tip–SAM distances), or a real difference in chain torsion or adsorption sites.[160,163] This remains an open question, especially taking into account that the multiplicity of structures is not observed by diffraction techniques.

In the last few years, attention has turned toward the $\sqrt{3} \times \sqrt{3}$ R30° lattice and the problem of the adsorption site. It was not until very recently that new models for the c(4 × 2) were proposed, which involve an important reconstruction of the surface and the presence of adatoms. These will be discussed in section 4.4. Moreover, the question of which of the structures, $\sqrt{3} \times \sqrt{3}$ R30° or c(4 × 2), is the more energetically favoured and how this depends on the chain length remains an open question.

4.3 Other surfaces structures

In addition to the dense $\sqrt{3} \times \sqrt{3}$ R30° and c(4 × 2) lattices and the more diluted lying down surface structures found at early stages of molecule adsorption, other lattices have been reported for alkanethiols on Au(111), mainly from STM measurements. Among them, striped phases with a completely different molecular structure than the lying down phases, also described as $p \times \sqrt{3}$, have been observed both in air and *in situ* in pure alkanethiol liquids. There has been some confusion about the orientation of the adsorbed molecules in some of these striped phases. In some cases, the origin of these structures is the existence of packed molecules with different α (*e.g.*, 50° instead of 30°),[174,175] or molecules placed at different sites.[170,172]

Another type of striped phase are the so-called "pinstripe" lattices which have been observed especially for short alkanethiolates on Au(111).[176,177] These phases consist of a $\sqrt{3} \times \sqrt{3}$ R30° lattice with periodically missing rows, a fact that is not surprising, considering that van der Waals interactions are relatively weak for SAMs of short molecules.

Rectangular phases, like the $(2 \times \sqrt{3})$ (0.6 nm × 0.5 nm), and $(4 \times \sqrt{3})$ (1.2 nm × 0.5 nm) lattices (Fig. 8a) have been imaged for propanethiolate,[54,152,154,155,178] and also for gently annealed (T = 60 °C) hexanethiolate SAMs.[118] On the other hand, local arrangements of tetramers with $(3 \times 4\sqrt{3})$[179] or (3×4)[180,181] periodicities have also been observed at low temperatures. In both cases the unit cells correspond to saturation coverage (θ = 1/3). All these rectangular structures evolve with temperature towards the $\sqrt{3} \times \sqrt{3}$ R30° or c(4 × 2) surface structures. Moreover, stable $7 \times \sqrt{3}$ and $5 \times \sqrt{3}$ have been observed by STM imaging for mercaptopyridine adsorption on Au(111).[182,183,184]

Some other interesting surface structures that deserve a detailed study and interpretation have been observed by STM. One of these structures is shown in Fig. 8b where stripes

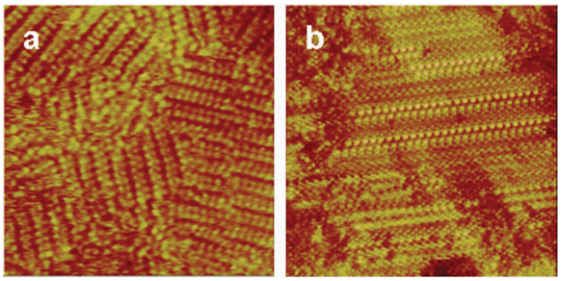

Fig. 8 STM images of hexanethiol lattices on Au(111) (a) (17. 9 nm × 17.9 nm) 4 × $\sqrt{3}$ rectagular lattice, (b) (30. 3 nm × 30.3 nm) striped domains of thiolate species with nearest-neighbour distances $2\sqrt{3} \times 2\sqrt{3}$.

of very bright spots with 2 × $\sqrt{3}$ nearest neighbour distances are observed superimposed on domains of the c(4 × 2) surface structure. Again, the problem of what is actually imaged by STM (the sulfur headgroups or the hydrocarbon chains) is present for these structures. Therefore, they should be analyzed by considering electronic and topographic effects: for example, by comparing experimental with STM images created from DFT calculations. And, once more, it is necessary to re-analyze the structures under the light of the new adatom models that we will review in the following section.

4.4 Is the Au surface reconstructed upon thiol adsorption? The new adatom models

Up to now, we have carefully avoided a discussion on the structure of the S headgroup–Au interface. This remains a controversial point even for the simple $\sqrt{3} \times \sqrt{3}$ R30° lattice. This point was initially addressed in the late 1990s by means of DFT calculations,[185–196] by considering the interaction of thiol molecules (usually methanethiol, or methane disulfide), with an unreconstructed Au(111) surface. Different adsorption sites were alternatively proposed as the energetically most favoured for alkanethiol adsorption. In fact, DFT calculations for methanethiolate on Au(111) performed by different research groups gave completely different results: hcp and fcc hollow,[197] bridge,[193] and the intermediate sites (fcc-bridge and hcp-bridge)[190–192] have all been regarded as the preferred sites for adsorption on the (111) surface. The reasons for this discrepancy could be differences in the calculation basis set, limitations in the calculation methods, or the presence of local energy minima. In the early 2000s this discussion stopped because the results from calculations of different groups started to converge: it seemed that for the $\sqrt{3} \times \sqrt{3}$ R30° alkanethiolate lattice the S headgroups were placed in equivalent sites somewhere between the fcc-hollow and the bridge sites (U model, Fig. 9).

However, more or less at the same time, XPD[198] and normal incidence XSW[199] studies of $\sqrt{3} \times \sqrt{3}$ R30° methanethiolate lattices on Au(111) formed from the gas phase showed an unexpected result: alkanethiolate adsorption would take place at on-top sites, the least favourable site among those usually considered in DFT calculations.[186–194] New GIXD results for dodecanethiolate SAMs on Au(111) were interpreted by considering the existence of incoherent domains of alkanethiolate molecules at on-top and fcc hollow sites on the

unreconstructed surface.[134] This two-adsorption site model tried to reconcile DFT calculations with experimental data by introducing kinetic considerations.

From that time on, several works have been published with new experimental data and theoretical models, both for the $\sqrt{3} \times \sqrt{3}$ R30° lattice and the c(4 × 2) lattice, that would indicate that thiol adsorption promotes a strong reconstruction of the Au(111) surface, with Au vacancies and/or Au adatoms playing a key role. For the $\sqrt{3} \times \sqrt{3}$ R30° lattice, Molina and Hammer[200] proposed a honeycomb surface structure with 1/3 Au atom vacancies in the outermost layer as the stable methanethiolate Au(111) lattice (R1, Fig. 9). Simultaneously, Morikawa *et al.*[201] proposed a model for the c(4 × 2) that included gold vacancy formation. As regards adatom models, Yu *et al.*[202] proposed one of the first ones for the $\sqrt{3} \times \sqrt{3}$ R30° (R2, Fig. 9) and c(4 × 2) lattices based on X-ray standing wave data. In all cases, a first Au layer involving 1/3 Au adatoms at fcc sites, with methanethiolate species chemisorbed on top of the gold adatoms (thus leading to RSAu species), was proposed. Additional support for this model was recently given by the same authors from XPS results.[203]

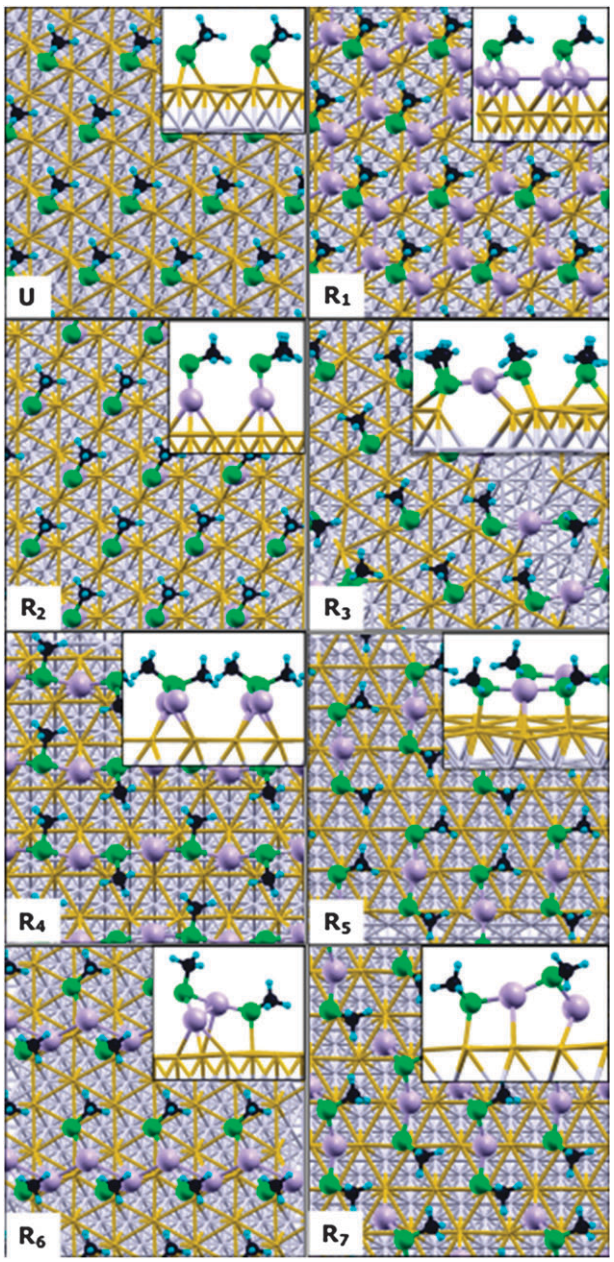

Fig. 9 Schemes for the $\sqrt{3} \times \sqrt{3}$ R30° and c(4 × 2) methanethiolate lattices on Au(111) for unreconstructed (U) and reconstructed Au surfaces: R1, R2, R3, R4, R5, R6, R7. The first gold layer (golden), Au adatoms (lilac), S atoms (green), C atoms (black), and H atoms (light blue) are shown. The insets show the lateral view.

On the other hand, new photoelectron diffraction and GIXD measurements for $\sqrt{3} \times \sqrt{3}$ R30° were interpreted by means of DFT-based MD calculations in terms of a dynamic equilibrium between bridge site adsorption and a novel structure where two CH_3S radicals were bound to a gold adatom that had been lifted up from the gold substrate (R3, Fig. 9).[204] This model was later extended to the c(4 × 2) surface structure, based on GIXD data for hexanethiolate on Au(111).[205]

In a different DFT study, Grönbeck and Hakkinen proposed a $(RSAu)_x$ polymer model (R4, Fig. 9), consisting of RS species bound to gold adatoms.[206] This so-called "divide and protect" idea has recently gained importance in view of some new results for the structure of thiol-protected gold nanoclusters.[120,207] Moreover, another group has recently suggested different gold–thiolate structures (dimers, oligomers, polymers) from DFT calculations.[208]

Grönbeck *et al.*[120] also proposed a different model for the c(4 × 2) surface structure from DFT data (R5, Fig. 9) that involves RS–Au–SR units ($(RS)_2Au$) in a *cis* configuration. However, in this case, the model does not include the dynamics equilibrium discussed in model R3.[209]

Moreover, two additional recently proposed models are presented. One of them (R6 in Fig. 9) is a chain structure made of RS–Au–SR complexes linked by gold adatoms.[210] The other one involves two adatoms per unit cell, with one of the adatoms in an fcc hollow and the other one in a bridge site (R7, Fig. 9).[211] As most of these models have been presented in the last three years, it is evident that the study of the nature of the thiolate–Au(111) interface is a very active (and attractive) research field, and that still no conclusions can be definitively drawn.

4.4.1 Experiments *vs.* models: the controversy. Models containing $(RS)_2Au$ complexes (R3, R5 in Fig. 9) became popular after STM imaging of diluted phases of methanethiolate[211] and benzenethiolate[212] in UHV at low temperature, which were interpreted in terms of RS–Au–SR species. However, it is difficult to directly extend conclusions from the diluted to the dense standing up phases. Note that, in contrast to the diluted phases, it is not possible to obtain direct evidence of the Au–S headgroup interface by STM imaging (Fig. 7a,b), because, in principle, one could image the end group of the hydrocarbon chain. Surface analysis techniques should give evidence about the organization of this complex interface. However, these techniques have given rise to conflicting results. In fact, vacancy, RSAu and $(RS)_2Au$ models seem to be either supported or refuted by experimental data, depending on the research group. For instance, the

R3 model (Fig. 9) involves bridging of one thiolate, while no evidence of bridging has been observed from combined X-ray standing waves and XPD data.[213] In addition, XPS results from the same group have shown that for methanethiolate on Au(111) the system can be well described by the RSAu model (R2, Fig. 9), rather than by the $(RS)_2Au$ models, although the authors admit that this seems to be valid only for this very short thiol.[203] On the other hand, the $(RS)_2Au$ model (R5, Fig. 9) seems to be supported by XRD data of thiolate-capped Au nanoparticles, which show the presence of two thiolates bonded to Au adatoms.[214] Finally, the vacancy model (R1, Fig. 9) does not seem to be compatible with diffraction data.[211] Therefore, the failure of surface analysis techniques to unambiguously solve the interface structure for thiolate SAMs has revitalized both STM (to obtain indirect evidence about interface organization) and DFT calculations (to explore the stability of the different models) as important tools to clarify this problem. In the next two sections we will discuss the adatom models in the light of theoretical calculations and indirect evidence from STM data.

4.4.2 The thermodynamic stability of the surface structure models. As regards DFT calculations, the large value for the adsorption energy of thiols on Au(111) is usually invoked as the driving force for the substrate reconstruction and is also employed to justify the corresponding stability of the phases. Although some comparison of energies for the different models has been reported[206,211] a careful theoretical comparison between relative stabilities of the proposed models is highly necessary. However, this is far from being straightforward because the models involve different surface unit cells. This fact precludes a direct comparison based on adsorption energies obtained from total energies (Table 2), since the former will not take into account the different stability of the reconstructed surfaces.

The surface free energy defined by Reuter and Scheffler[215] provides a more physically grounded way to predict the relative stability of thiolate lattices on metal surfaces than the adsorption energy.[87,215,216] The surface free energy is defined in the usual way ($\gamma(\Delta\mu) = \frac{\Delta G}{A}$), ΔG being the Gibbs free energy for the formation of the phase and A the area of the unit cell. In the case of the different models for methanethiol adsorption presented in Fig. 9, the gold surface is considered to be in contact with a $(CH_3S)_2$ gas phase at a given pressure and temperature. By defining the chemical potential of the adsorbate with respect to the $(CH_3S)_2$ molecule as $\Delta\mu = \mu - \frac{1}{2}g_{(CH_3S)_2}, g_{(CH_3S)_2}$ being the Gibbs free energy of the dimethyl disulfide, one can implicitly include P and T.[215] The above definition of $\Delta\mu$ allows an expression to be written for the surface free energy of the total system ($\gamma(\Delta\mu)$), which takes into account the amount of $(CH_3S)_2$ in the gas phase as:

$$\gamma(\Delta\mu) = \frac{1}{A}[E^{CH_3S/Au} - N_{Au}E^{Au}_{Bulk} - N_{CH_3S}\Delta\mu] - \gamma_{clean} \quad (4)$$

where $E^{CH_3S/Au}$ is the total energy of the adsorbate-substrate system. N_{Au} and E^{Au}_{Bulk} are the number of Au atoms in the slab unit cell and the total energy of bulk Au, respectively, and γ_{clean} is the surface free energy of the unreconstructed Au(111) surface, which has to be subtracted due to the asymmetry of the slab models.

Therefore, we will analyze the thermodynamic stability of the models shown in Fig. 9 following the approach described in ref. 87, 216. In Fig. 10 the surface free energy $\gamma(\Delta\mu)$ is plotted as a function of the methanethiolate chemical potential ($\Delta\mu$) with respect to the dimethyl disulfide (no adsorption takes place from methanethiol, as discussed in section 3) both for unreconstructed Au(111) and for the different reconstructed models. Note that U, R1, R2, R3, and R4 correspond to the $\sqrt{3} \times \sqrt{3}$ R30° lattice, while R5, R6 and R7 are applicable to the c(4 × 2) superlattice. In all cases the C–S–Au angle approaches that expected for a S sp^3-like hybridization.

From the point of view of gold chemistry, Fig. 10 clearly shows that the models containing RSAu complexes (R2, R4, R6 and R7) are thermodynamically less stable than the one that contains only $(RS)_2Au$ species (R5). The R2 model is also unstable with respect to thiolate adsorbed on the unreconstructed Au(111) surface (U model), while R4 and R7 have a similar stability to the U model. The best stability

Table 2 Adsorption energy (E_{ad}), Bader charge, Work function relative to Au(111) (ΔW), and surface dipolar moment (Δd) for the different models shown in Fig. 9

		Bader Charge/e			
Model	E_{ad}/eV	S atom	Au adatom	ΔW/eV	Δd/D
U	−1.82	−0.2	+0.05[c]	−1.5	−0.9
R_1	−2.61	−0.13	+0.07	−1.0	−0.6
R_2	−2.20	−0.13	+0.14	−1.0	−0.6
R_3	−1.89	−0.15[a]	+0.12	−1.44	−0.87
		−0.11[b]	+0.06		
R_4	−2.48	−0.17	+0.14	−1.15	−0.69
R_5	−2.34	−0.14	+0.14	−1.2	−0.72
R_6	−2.32	−0.17[a]	+0.12	−1.48	−0.89
		−0.12[b]	+0.08		
R_7	−2.43	−0.18[a]	+0.15	−1.12	−0.67
		−0.11[b]	+0.06		

[a] Stands for methanethiolate adsorbed in non equivalent adatoms. [b] Stands for methanethiolate adsorbed in non equivalent adatoms. [c] Stands for an Au surface atom.

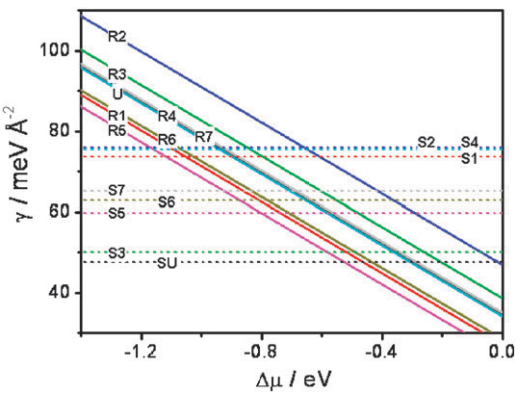

Fig. 10 Surface Gibbs free energy $\gamma(\Delta\mu)$ *vs.* CH_3S chemical potential ($\Delta\mu$) with respect to dimethyl disulfide for methanethiolate on an unreconstructed Au(111) surface (U) and on different models for reconstructed surfaces (R1–R7), The dotted horizontal lines indicate the surface free energy of the clean unreconstructed Au(111) (SU) and of the different clean reconstructed surfaces (S1 to S7).

among RSAu models is obtained for R6, which is clearly more stable than the unreconstructed Au(111) surface, but remains more unstable than the R5 model involving $(RS)_2Au$ moieties. Note that the R3 model, which exhibits both $(RS)_2Au$ species and methanethiolate bound at bridge sites, is slightly less stable than the U model. Concerning the surface structures, the R1 model involving vacancy islands is the most stable for the $\sqrt{3} \times \sqrt{3}$ R30° methanethiolate lattice. On the other hand, the surface free energy of R5 model, which is solely based on $(RS)_2Au$ species, is the lowest among the structures proposed for the c(4 × 2) superlattice. Finally, when comparing the stability of the $\sqrt{3} \times \sqrt{3}$ R30° *vs.* that of the c(4 × 2) lattices, we note that R5 exhibits a slightly better stability than model R1. The stability of model R5 arises from two separate contributions: (a) the model requires only a small amount of adatoms (0.17) (b) the S headgroup is not only attached to the Au adatoms, but also interacts with the Au surface (as shown in Fig. 9), leading to a large adsorption energy (Table 2). On the other hand, the highest instability of model R2 results from the large energy needed to obtain a 0.33 adatom coverage, which is not compensated for by the high adsorption energy on the reconstructed surface (Table 2).

In conclusion, from the point of view of thermodynamic stability the $(RS)_2Au$ and vacancy models are good candidates for explaining alkanethiolate c(4 × 2) and $\sqrt{3}\times \sqrt{3}$ R30° surface structures on Au(111), respectively.

4.4.3 STM imaging. We will now discuss the previous models under the light of experimental data. While calculated GIXD patterns for the R5 ($(RS)_2Au$) model are in reasonable agreement with the experimentally observed data, the calculated STM images are not consistent with the experimental images of the c(4 × 2) structure.[211] In fact, the calculated images exhibit a slight deviation from ideal packing structure, resulting in the typical pattern for the c(4 × 2) lattice with ~0.1 Å height modulation, which is significantly smaller than the 0.4–0.7 Å observed experimentally. As concluded by these authors[211] the $(RS)_2Au$ model requires a disruption of the ideal packing to be compatible with the c(4 × 2) STM images. Note, however, that in that work it was assumed that the STM images were dominated by topography and that electronic contributions were not relevant, a fact that still has to be demonstrated. In order to solve this problem the same authors[211] proposed model R7, which includes two adatoms per unit cell (Fig. 9), where one of the adatoms is in the fcc hollow and the other is placed in the bridge position. This structure exhibits a height modulation which brings about simulated STM images closely resembling those experimentally observed for the c(4 × 2) surface. However, according to our calculations (Fig. 10), this model is also unstable compared to the $(RS)_2Au$ models.

On the other hand, in some STM and AFM studies in air, real-time transformations from the $\sqrt{3} \times \sqrt{3}$ R30° lattice to the c(4 × 2) lattice had been reported, and thus for some time it was believed that the latter was the most stable structure on Au(111).[217] However, Terán Arce *et al.*[218] reported that the structural dynamics of alkanethiol monolayers on Au(111) showed reversible $\sqrt{3} \times \sqrt{3}$ R30° ⇔ c(4 × 2) transitions both in air and in pure thiols. Moreover, *in situ* STM results of hexanethiolate SAMs taken in 0.1 M NaOH aqueous solutions have revealed the existence of the same reversible $\sqrt{3} \times \sqrt{3}$ R30° ⇔ c(4 × 2) transformations.[219] These transformations are independent of the applied potential within the potential range where SAMs are stable. Although the interaction of the STM tip with the alkanethiolate SAM would also provide the necessary energy to go from one structure to the other, it is evident that they interchange easily. Since adatoms present in the surface cannot escape into the metal bulk, and can only disappear by attaching to a step edge, the $\sqrt{3} \times \sqrt{3}$ R30° and c(4 × 2) lattices should contain the same amount of adatoms. It has been considered that is impossible to form a $\sqrt{3} \times \sqrt{3}$ R30° phase from $(RS)_2Au$ complexes.[211] However, very recently, dilute and dense intermediate phases observed during methanethiolate self-assembly on Au(111) have been imaged at ~5 K.[179] The images have been interpreted in terms of the $(RS)_2Au$ moieties. The authors have also proposed that the adatom complexes can form local arrangements with the $3 \times 4\sqrt{3}$ or 3 × 4 unit cells, both providing the saturation coverage of CH_3S species on the Au(111) surface. They proposed that, by introducing long range disorder into the $3 \times 4\sqrt{3}$ phases at near-saturation coverages, one can obtain the macroscopically averaged GIXD pattern of the $\sqrt{3} \times \sqrt{3}$ R30° lattice. Upon *trans–cis* isomerization of the constituent of the $(RS)_2Au$ complexes, the $3 \times 4\sqrt{3}$ phase could attain the c(4 × 2) structure of the longer alkanethiolates.

In conclusion, the adatom model involving $(RS)_2Au$ moieties for the c(4 × 2) lattice seems to be well grounded both from GIXD data and from the point of view of theoretical stability, but many experimental observations, such as STM contrast, still have to be explained. An additional problem is to explain the $\sqrt{3} \times \sqrt{3}$ R30° structure in terms of the $(RS)_2Au$ species.

4.4.4 The fate of the adatoms after SAM desorption. Thiol adsorption/desorption measurements could provide indirect evidence about the presence of thiolate–Au complexes in the SAMs. In fact, if these species are present in the SAMs, thiolate removal should release free Au adatoms that in turn should rearrange on the surface in order to decrease the surface free energy of the system. The mobile Au adatoms produced by the thiolate removal process would then have two possibilities: (1) they could be incorporated at step edges; or (2) they could nucleate forming gold islands. The latter process should be preferred at large terraces. Nucleation of Au adatoms to form nanometre-sized islands has been observed by STM during the lifting of the herringbone Au(111) surface reconstruction. In this case the extra surface atoms present in the $22 \times \sqrt{3}$ structure are expelled, and nucleate to form Au islands of monoatomic height.[220] Therefore STM imaging of large terraces after thiolate removal could provide indirect evidence about the presence of thiolate–Au complexes through the observation of island formation. Moreover, the island coverage should give an idea about the stoichiometry of the complex.

STM measurements of this kind have been performed *in situ* on Au(111) terraces during the removal of a dense octanethiolate SAM (θ = 1/3) exposed to hydrogen atoms.[221] The authors

showed that, after SAM desorption, islands few nanometres in size and 0.24 nm in height are formed on the substrate surface.[221] Assuming that these bright features corresponded to Au islands, since their height is consistent with the height of monoatomic Au islands formed by the reaction

$$n(RS)_2\text{–Au} + 2n\text{H} \rightarrow 2n\text{RSH} + \text{Au}_n \qquad (5a)$$

or by the reaction

$$n\text{RS–Au} + n\text{H} \rightarrow n\text{RSH} + \text{Au}_n \qquad (5b)$$

the measured surface coverage of Au atoms in the islands (θ_{adat}) should be 0.17 for reaction (5a) and 0.33 for reaction (5b). The experimental results lead to $\theta_{adat} \approx 0.17$,[221] a figure consistent with the presence of $(RS)_2$Au species, and therefore, supporting models R5 or R3 (Fig. 9). The authors also speculated that these structures should be the same as those observed after reductive desorption of thiol by electrochemical methods, although no evidence about the presence of the c(4 × 2) surface structures (for which the $(RS)_2$Au model is R5 strictly applicable) was given before SAM removal.

As mentioned above, STM measurements for alkanethiolate SAM desorption have been performed under electrochemical control.[222–225] Conventional electrochemical techniques, like cyclic voltammetry, are usually employed to characterize thiol SAMs in electrolyte solutions. In particular, reductive desorption curves (cathodic scans in the cyclic voltammograms) give information about the amount of adsorbed thiolates on the metal surfaces. A typical current density (j)/potential (E) profile for hexanethiolate desorption from the Au(111) surface recorded in 0.1 M NaOH is shown in Fig. 11a. The well-defined cathodic peak corresponds to the reductive desorption of the thiolate species from the Au surface, according to reaction[226]

$$\text{RS–Au} + e^- \rightarrow RS^- + \text{Au} \qquad (6)$$

The charge density (q) involved in these peaks allows an estimation[227] of the amount of chemisorbed thiolates on the Au surface. In fact, the value $q \approx 75$–$80\ \mu C\ cm^{-2}$, obtained from integration of the voltammetric peak, corresponds to a thiolate coverage $\theta \approx 1/3$, assuming one electron transfer for the reductive process (reaction 6).

In Fig. 11b the SAM structure with molecular resolution taken by *in situ* STM at an applied potential $E = -0.50$ V (*vs.* the saturated calomel electrode, SCE), *i.e.* before desorption, is shown. Indeed, in the $-0.8\ V < E < -0.4$ V potential range, the SAM structure was stable. Different rotated domains of the c(4 × 2) lattice can be observed in the image. Afterward, the potential was scanned from −0.50 V to −0.99 V, just at the reductive desorption peak (Fig. 11a). In the STM image (Fig. 11c) obtained at −0.99 V (the time difference between the images in Fig. 11b and c is 200 s) the rows of the c(4 × 2) structure are no longer observed, while a large number of nanometre-sized islands with average height 0.24 ± 0.03 nm are formed. Measurements for decanethiolate SAM desorption gave the same values. These islands were repetitively imaged for minutes under these experimental conditions, *i.e.* no island removal was observed. The size and the height of the islands are consistent with those reported by Kandel *et al.*[221]

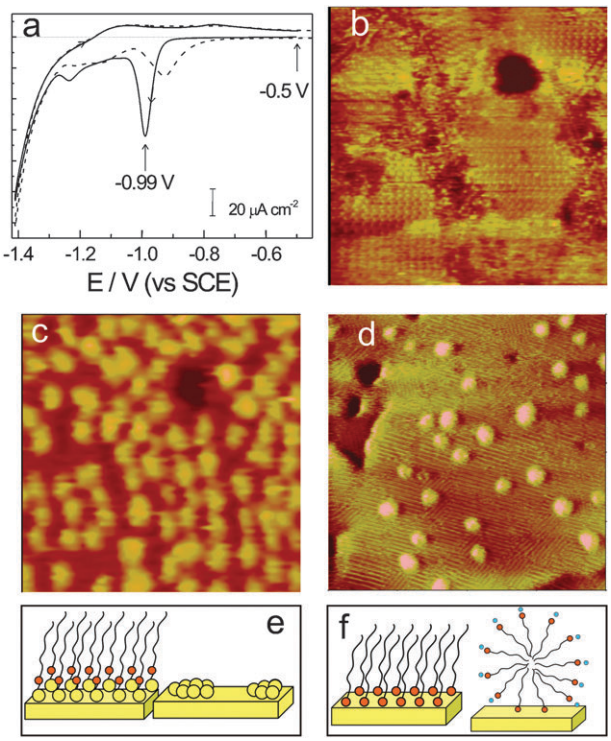

Fig. 11 (a) Reductive desorption curves in 0.1 M NaOH electrolyte: (—) first scan, (---) second scan. Scan rate was 0.05 Vs^{-1}. (b) 30 × 30 nm^2 *in situ* STM image (raw data) of hexanethiolate SAM on Au(111) taken at −0.5 V (arrow in (b)) in 0.1 M NaOH. (c) 30 × 30 nm^2 *in situ* STM taken at the same region as (b) after 200 s at $E = -0.99$ V (see arrow in (a)). (d) 80 × 80 nm^2 STM image of hexanethiol after soft annealing in ethanol. Schemes showing (e) the formation of Au islands for the RSAu model and (f) thiolate micelles for desorption from an unreconstructed Au(111) surface.

Assuming that reductive desorption takes place by reactions

$$n(RS)_2\text{–Au} + 2ne^- = 2nRS^- + \text{Au}_n \qquad (7a)$$

or

$$n\text{RS–Au} + ne^- = nRS^- + \text{Au}_n \qquad (7b)$$

the θ_{adat} should give an indication of the type of thiolate complexes present on the Au surface, as discussed before. However, in contrast to that found during hydrogen desorption, the fraction of the area covered by the islands in the STM images under electrochemical control results in $\theta_{adat} = 0.30$–0.40 (Fig. 11c), *i.e.* much larger than the $\theta_{adat} = 0.17$ (reaction 7a) expected for the $(RS)_2$Au model[120] and also slightly higher than the $\theta_{adat} = 0.33$ value expected for the RSAu model (reaction 7b).[228]

Similar islands were observed during soft annealing ($T = 60\ ^\circ C$) in ethanol of the SAMs, which leads to partial desorption of thiolates (Fig. 11d). The image shows islands coexisting with domains of lying down alkanethiolate molecules.

On the other hand, the islands shown in the STM images after desorption experiments could be assigned to RSH aggregates that remain physisorbed on the Au surface, or, in the case of reductive desorption in aqueous electrolytes, to the formation of RS^- micelles.[219,229] Desorption processes leading

to Au islands and thiolate micelles are schematically shown in Fig. 11e,f. Also, it is possible that the features imaged by STM correspond to a mixed situation: thiolates adsorbed at the edges of Au islands. Moreover, it has also been shown that hyperthermal proton ion bombardment (2–6 eV) of dodecanethiolate SAMs leads to the formation of a large number of nanometre-sized islands that have been assigned to aggregates formed by cross-linked molecules with some S–Au bonds and unreacted thiol molecules.[230] Although the nature of these structures has not yet been completely clarified, the intriguing fact is that the aggregate height is always close to that expected for Au islands.

4.4.5 The origin of adatoms during self-assembly. It is clear that, if thiolate–Au complexes are formed, Au adatoms should come from the Au surface by some kind of erosion/etching/ejection process taking place at step edges or at terraces. In fact, in addition to the $\theta_{adat} = 0.05$ supplied by the lifting of the $22 \times \sqrt{3}$ surface reconstruction an additional 0.12 (or 0.28)[221] surface coverage of gold adatoms is needed to form a dense thiolate lattice ($\theta = 0.33$) formed by $(RS)_2Au$ (or RSAu) complexes. The formation of Au adatoms could be responsible for the well-known vacancy islands (or pits) (dark hole in Fig. 11c), which will be also discussed in Section 5.1. However, it is evident that the small area of this vacancy island (surface coverage $\theta_{vac} = 0.05$, depth 0.24 nm) cannot account for the $\theta_{adat} = 0.12$ needed to form dense thiolate lattice of $(RS)_2Au$ species (and even less for the $\theta_{adat} = 0.28$ necessary for RSAu species).

We have made a systematic analysis of large scale STM images of SAM-covered terraces (typically larger than 100×100 nm^2), where the contribution of adatoms coming from step edges should not be important. As an example we show in Fig. 12a a typical image for a nonanethiolate SAM that exhibits $\theta_{vac} = 0.20$. The distribution function of θ_{vac} for different alkanethiolate SAMs derived from more than 50 STM images ranges from 0.05 to 0.40, as shown in Fig. 12. Despite the fact that the histogram is very broad, the maximum at $\theta_{vac} \approx 0.1$ seems to be consistent with the $(RS)_2Au$ model, in agreement with previous results.[179] Note, however, that θ_{vac} was obtained under the assumption that the vacancy islands are always monoatomic in depth, although in some cases the pits are deeper (two atomic layers in depth), which would lead to a larger number of available adatoms.

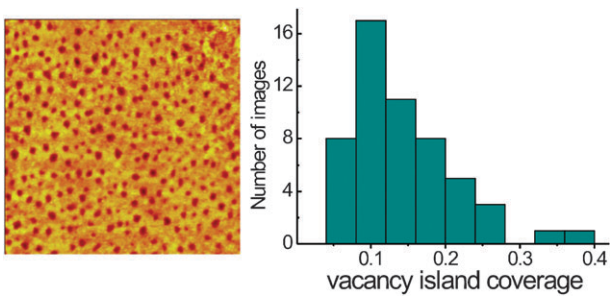

Fig. 12 140×140 nm^2 *ex situ* STM image of a large (111) gold terrace covered with a nonanethiolate SAM. The dark regions correspond to vacancy islands. The histogram corresponds to the distribution of vacancy island coverage from 56 STM images ($\sim 100 \times 100$ nm^2) of different alkanethiolate SAMs.

There are also other interesting observations that still require explanation in terms of adatom models. In fact, during the formation of densely packed domains of the $c(4 \times 2)$ for 4-methyl-4′-mercaptobiphenyl on Au(111), small islands are unexpectedly seen on the Au substrate instead of the etch pits commonly observed after formation of organothiolate adlayers,[146] and which are regarded as the most likely source of adatoms. The same has been found for other arenethiols.[231,232]

After reviewing the desorption/adsorption experiments, some conclusions can be drawn. It is clear that desorption of $c(4 \times 2)$ domains results in island or aggregate formation.[219,221] However, if one assumes that the islands are formed by the gold adatoms produced from the removal of the adatom–thiolate moieties, the experimental results from gas phase or from electrochemical removal cannot give a conclusive answer related to the thiolate–gold complex stoichiometry. Therefore, in order to correlate thiolate surface structures with models, more experimental and theoretical work is still needed.

Finally, it should be noted that another adatom source for Au–thiolate complexes could be step edges. Since the energy to form an adatom from these sites is lower than that required to remove an atom from a terrace, some of the thermodynamically unstable models considered in Fig. 9 and 10 can become stable.[211] However, as shown in Fig. 12, vacancy islands are also formed on smooth terraces, so that the models should be thermodynamically compatible with Au–thiolate complex formation on atomically smooth, defect free Au(111) surfaces, as considered in the DFT calculations.

5. The quality of self-assembled monolayers on Au(111)

5.1 Structural defects

In many of the schemes usually found in the literature, especially when dealing with nanotechnological applications, SAMs on gold are sketched as perfect monolayers, with molecules in a closed packed configuration. However, this idea is far from real. In fact, there are several types of defects that can have an important influence in the efficiency of some of the applications, such as in the case of sensors and in nanomolding and nanoreplication. These defects are typically found for alkanethiol, alkanedithiol and arenethiol SAMs, even on single crystal Au(111) surfaces. Some strategies can be employed to minimize them, but it is important to take into account that they will always be present to a certain extent. In this section we will briefly describe some of these defects at the molecular level.

Molecular defects are present even in well-ordered, crystalline alkanethiolate domains (Fig. 13). These defects can be either a small number of missing molecules (also called pinholes) (Fig. 13c), or regions where the molecules have a certain degree of disorder. In this second group we can find totally disordered, liquid-like domains, regions with well-packed molecules that have a different α, or domains

with molecules whose hydrocarbon chains are not fully extended.

On the other hand, the commensurate molecular layer can adopt a number of symmetry-equivalent registries with respect to the Au lattice. Under growth conditions where the distance between nucleation centers is smaller than the terrace size, various domains nucleate, grow, and coalesce with formation of a network of domains. Each domain is formed by an ordered arrangement of alkanethiol molecules with identical packing and coherence within a single domain. The domains are separated by boundaries of molecular scale dimensions (bright fissures between domains). The boundary is a defective region in a SAM, as shown in detail in Fig. 13b. Either if there are adjacent domains of different lattices (*e.g.*, $\sqrt{3} \times \sqrt{3}$ R30° and c(4 × 2)), or two domains of the same ordered lattice with a different χ (Fig. 3), the domain boundary consists of mismatching (or simply missing) molecules. Most boundaries are observed to have three orientations originating from the hexagonal Au(111) three-fold surface symmetry, due to the remarkable degree of epitaxy that alkanethiol SAMs have with Au(111) surfaces.

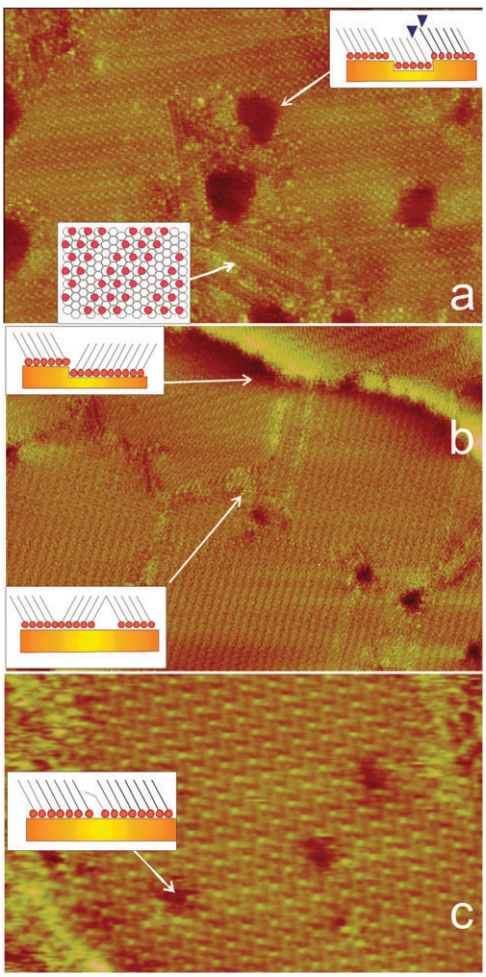

Fig. 13 STM images of alkanethiolate SAMs on Au(111) showing different types of surface defects (sketched in the insets) (a) vacancy islands and missing rows (48 × 32 nm^2 image), (b) domain boundaries and step edges (46 × 33 nm^2 image) (c) molecular defects (pinholes) (19 × 12 nm^2 image).

Another type of defect are rows of missing molecules, which are especially found for short alkanethiols (Fig. 13a), since chain–chain interactions are smaller, which has been already mentioned in Section 4.3. Two types of missing rows have been observed: straight and zig-zag.[233] Surface structures with missing rows can also be found as a result of some SAM annealing procedures together with lying down phases.

On the other hand, the large black regions in Fig. 13a are not real SAM defects. For SAMs formed both from the gas phase and from solution it has been seen by STM and AFM, that during self-assembly gold 2D vacancy islands of monoatomic (0.24 nm) or diatomic (0.48 nm) depth are formed whose base is covered by alkanethiolate molecules.[117,128,234,235] At first it was though that the origin of these pits was the removal of some gold atoms (which would go to solution) due to a weakening of the Au–Au bonds caused by the presence of the adsorbed alkanethiolate. However, even if a small amount of gold has been detected in the incubation solutions,[235] the amount was not enough to explain the pits. Moreover, since these features are also formed for gas phase alkanethiolate SAMs, the most reliable theory is that they are produced by some kind of substrate reconstruction. In the light of the new adatom models it is plausible to consider them a source of adatoms, as discussed in previous sections. Whatever their origin is, it has been reported that pit density increases with increasing alkanethiol concentration, and decreases with increasing length of the hydrocarbon chain.[235] Moreover, in addition to vacancy islands, gold substrates (even single crystals), have other structural defects, like steps (Fig. 13b) and dislocations and, in the case of polycrystalline Au films, intergrain boundaries, which in turn produce defects in the SAMs.

5.2 Chain ordering

Thiol SAMs can exhibit both a positional order, fixed by the headgroup–Au adsorption energy, and orientational order, fixed by the hydrocarbon chain interactions.[236] Positional order does not necessarily imply the existence of orientational order because the gold–sulfur adsorption energies (see Table 2) are much higher than the van der Waals forces between hydrocarbon chains (~0.05 eV per C atom). Therefore, it is possible to have the S headgroups forming ordered lattices and yet have orientational and conformational disorder in the hydrocarbon chains.[237]

Ordered alkanethiolates in SAMs tend to adopt a crystalline-like, all-*trans* configuration. This issue has been explored by using IR spectroscopy techniques, such as IRRAS and PMIRRAS. Well-ordered, crystalline alkanethiolate monolayers on metal substrates display peaks corresponding to the methylene asymmetric $\nu_{as}(CH_2)$ (d^-) and symmetric $\nu_s(CH_2)$ (d^+) stretching modes at about 2920 cm^{-1} and 2850 cm^{-1}, respectively (Fig. 14a).[238] Some differences have been found for alkanethiolates with odd and even numbers of CH_2. Moreover, the presence of the methyl stretching mode ($\nu_{as}(CH_3)$) at 2975 cm^{-1} is a clear indication that the methyl end groups are oriented. Among these bands, d^- is taken as the reference to measure the degree of ordering of the hydrocarbon chains. A close inspection of this band indicates that it

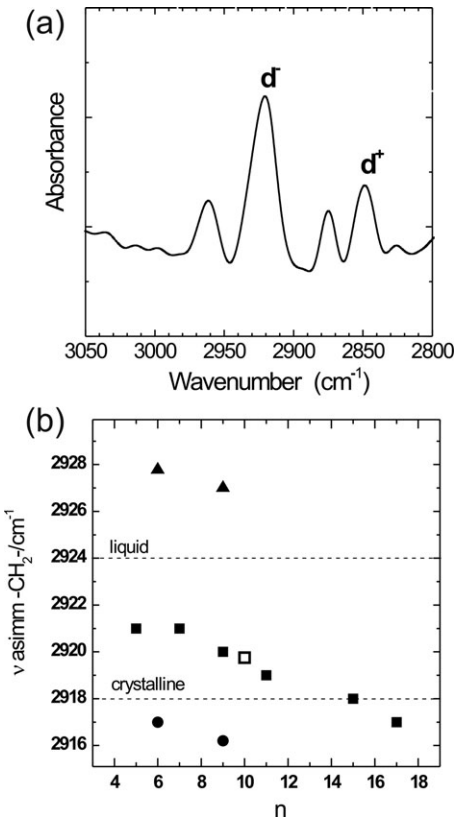

Fig. 14 (a) Typical methyl and methylene IR stretching region for decanethiolate adsorbed on Au(111). d^+: $\nu_s(CH_2)$; d^-: $\nu_{as}(CH_2)$; (b) The position of d^- *vs.* the number of carbon atoms for: (■) (□) alkanethiolates on Au(111); (●) alkanedithiols on Au(111) prepared from hexane solutions; (▲) alkanedithiols on Au(111) prepared from ethanolic solutions. Dashed lines correspond to the position of the d^- band measured for a liquid and for a crystalline solid alkanethiol. Data taken from Reference 125 and 238 with permission of the American Chemical Society.

can be deconvoluted into two components: the first one, below 2920 cm^{-1}, is the result of ordered domains of the monolayer, while the second one, above 2920 cm^{-1}, corresponds to the disordered domains of the monolayer.

Increasing the temperature (up to 348 K) produced a shift in the position of both $\nu_{as}(CH_2)$ and $\nu_s(CH_2)$ modes to higher wavenumber ($\sim$4 cm^{-1}), while their peak widths broadened. This means that a significant number of *gauche* defects are created during the thermal treatment, and that the film is no longer closely packed, *i.e.* the amount of "disordered" domains increases on the surface.[111] On the other hand, the rapid decrease in intensity of both methyl and methylene modes when the SAM is heated at temperatures greater than 348 K implies monolayer decomposition.

The ordering of the hydrocarbon chains depends markedly on the adsorption time, hydrocarbon chain length, the nature of the terminal groups, the temperature and the substrate quality, among other variables. As shown in Fig. 14b the degree of order, estimated from the position of the d^- band, gently increases when the hydrocarbon chain length (n) is increased. For $n > 18$ it is considered that the crystalline-like, all-*trans* state is approached, while for $n < 8$ the SAMs are in a disordered state, as shown in Fig. 14b. However, even long-chain SAMs are not perfectly crystalline, as revealed by He diffraction measurements at 298 K, which show that the chain ends are highly mobile.[239]

Chain ordering in alkanethiolate-capped gold nanoparticles 2–3 nm in diameter has also been studied.[240] It has been found that, for long chain thiols, the alkyl chains exist predominantly in an extended, all-*trans*, ordered conformation at 298 K. Calorimetry, variable temperature transmission FTIR spectroscopy, and solid state ^{13}C NMR studies have established that a cooperative chain melting process occurs, although it is not immediately evident how this process takes place, given the relation between the extended chain conformation and the geometry of the spherical nanoparticles. TEM images reveal that adjacent gold particles are separated by approximately one chain length, suggesting that chain ordering arises from an interdigitation of chains on neighbouring particles. Electrochemical thermograms[236] have shown that long chain alkanethiolate SAMs (n = 16, 18, 20) on planar Au and gold nanoparticles exhibit a crystalline-to-liquid transition at temperatures that increase with chain length (312 $K \leq T \leq$ 337 K). In that work it was also shown that the transition temperatures are in the range for those observed for the related phospholipids in bilayers.[236]

On the other hand, the introduction of terminal groups (–SH, –COOH, –OH, $–NH_2$) different from the $–CH_3$ group usually results in a decrease in SAM ordering.[164] Similar results have been observed by introducing benzene rings in the hydrocarbon chains.[241] However, it has been found that short CH_3-terminated alkanethiols are disordered at 300 K, while similar COOH-terminated thiols are crystalline up to 415 K.[242] A slight increase in the order–disorder transition temperature for OH-terminated (with respect to CH_3-terminated thiols) has also been reported.[243] In these cases the ordering has been assigned to hydrogen bond formation. Therefore, the effect of the terminal group on chain ordering (hydrogen bonding, electrostatic interactions) is not completely clear. In particular the effect of solvent, pH and substrate topography should be carefully investigated.

5.3 Improving SAM quality

Several strategies can be employed to improve the quality of thiol and dithiol monolayers on Au(111). A careful choice of the solvent and of the self-assembly conditions can yield SAMs with lower defect density and better chain ordering.[2] Monolayers of alkanethiols with varied chain lengths have been prepared from pure thiols and from solutions in solvents like ethanol and hexane.[2,72,244]

The self-assembly conditions are even more important for dithiol SAMs. In fact, it has been observed that self-assembly from ethanolic solutions promotes multilayer[245] and disulfide or sulfonate formation by oxidation of the end group (see also Section 6.3).[223,246,247] On the other hand, self-assembly from hexane solutions performed in the dark and in the absence of oxygen produces dense, well-ordered SAMs of dithiols in standing up configuration.[115] At present, it is not clear if oxygen and ethanol promote intrachain-disulfide formation or if disulfides are formed by addition of more dithiol

molecules to the SAMs. While XPS is not able to unambiguously detect disulfide bond formation in the SAMs (the S 2p signal for disulfides is at the same position as for free dithiols (163 eV), see section 6.1), electrochemical measurements for hexanedithiol SAMs give an excess of charge for the SAM reductive desorption peak[115] which has been related to the electrons needed to reduce the disulfide bonds formed at the end groups of the SAM.[246]

In the case of solution adsorption, increasing the solution temperature to 50–70 °C (depending on the solvent),[61,167,248,249] or soft annealing of the SAMs (T = 50–100 °C) formed at room temperature, either in air or in UHV,[62,117,234] have been all proposed as a means to reduce the number of defects and as a strategy to obtain larger ordered domains of thiols and dithiols. However, while SAM annealing in air or UHV lowers the number of defects, it also produces missing rows or lying down phase domains.

Some other good strategies to obtain well-ordered SAMs include the formation of SAMs at controlled potentials[250] and repeated immersions of the substrates followed by voltammetric cycles.[71,72] In general, annealing in solution and repetitive voltammetry and immersion seem to improve the monolayers, although none of these procedures really yields a defect-free monolayer. However, other studies[63,64] claim that SAMs formed at controlled potentials behave very similarly to the monolayers adsorbed from thiol solutions or pure thiols as far as stability and structural orientation are concerned, irrespective of the chain length.[244]

5.4 Impact of SAM quality in applications

For many SAM applications the quality of SAMs prepared under "standard" conditions is enough, but, for others, defects are a serious problem, and the control of the SAM quality is a crucial point. A typical example for which high-quality SAMs are required is in the field of electronics and spintronics. Although alkanethiolate SAMs are certainly not the best candidates for these applications (due to their high mobility and low conductance), similar defects as those shown in Fig. 13 are also present in the more "promising" phenyl- and non-saturated thiol and dithiol SAMs.[66]

In the case of molecular electronics and spintronics, metallization of the thiol SAMs is often needed to build different types of devices. However, during metal deposition (from physical vapor deposition, chemical vapor deposition or electrochemistry), defects and chain disorder enable the diffusion of metal species, connecting the deposited metal layer with the substrate, and thus leading to inefficient systems (Fig. 15a).[251,252] Degradation of the SAM quality during thermal vapor deposition has also been observed, in agreement with experimental results of the previous sections. The "top-contact problem" is one of the biggest problems in the fabrication of molecule-based devices. Different strategies have been developed to minimize this problem, including SAM polymerization by electron irradiation before metallization,[253] exposure of –SH,[254] –OH or –COOH terminated SAMs to metal organic precursors,[255] among others.[251]

Defects are important for the understanding of charge transfer through SAMs. In fact, many charge transfer studies

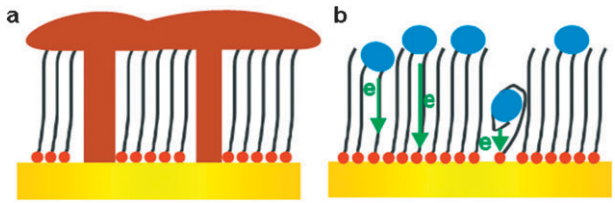

Fig. 15 Impact of SAM defects on the applications: (a) Scheme showing the "top-contact" problem in thiol-based electronic devices. The metal deposit (brown) penetrates the SAM at pinholes. (b) Changes in charge transfer mechanisms for adsorbed redox molecules (blue) due to structural defects (pinholes) and changes in chain ordering.

have focused on tunnelling mechanisms through the hydrocarbon chain.[256] However, when defects are present, they can be an alternative path for charge transfer (Fig. 15b). For instance, electrochemical measurements of Au(111) substrates modified by alkanethiols with different chain lengths and terminal groups in methylene blue (MB) solutions have revealed that the MB redox couple is reversible, independent of the alkanethiol chain length or the terminal group.[177,257] This evidence, and the fact that the charge transfer was hindered when the defect density was reduced by gentle annealing in solution, lead to the conclusion that, at least in some cases, electron transfer occurs through defects, and not by a tunnelling mechanism through the insulating alkanethiolate SAMs.[177,257]

High quality SAMs are also required for the preparation of hybrid phospholipid membranes, which consist of an inner alkanethiolate SAMs and an outer phospholipid layer.[2,258] Most of these structures are built for electrochemical sensing of species by specific channels, and, thus, extremely low capacitance values are required. Therefore, the inner alkanethiolate layer should have domains with highly ordered chains and a low defect density.

As regards nano/micropatterning techniques, including dip pen nanolithography,[259] microcontact printing,[260] edge spreading lithography[261] and microdisplacement printing,[262] they all require a strict control of the diffusion of the molecular "ink" on the underlying SAM. This is needed for the creation of strictly-bounded, high-resolution nanopatterns with minimized ink "spreading" and limited "smudging" at pattern boundaries. SAM defects, such as domain boundaries and high density of vacancy islands, could have a strong influence on ink spreading. SAMs of different alkanethiols, formed by contact printing and solution adsorption, have been characterized by IRRAS and electrochemical impedance spectroscopy (EIS).[263] While the contact printed monolayers seem to be structurally similar to those prepared by solution adsorption, as evaluated by IRRAS, EIS results provide evidence that the two result in different interfacial properties: the former are less resistive to charge transfer and have greater defect density than those prepared by solution adsorption. For the contact printed monolayers it has also been reported that the density of defects decreases with increasing solution concentration.[263]

From a positive point of view, defects at SAMs can be used to build nanocontacts and to prepare small metallic nanoclusters by confined growth at defects.[113] Moreover, different

kinds of hydrophobic and lipophilic molecules can be easily immobilized on highly disordered SAMs. In fact, thiolate-covered Au nanostructured substrates can be used to trap molecules, to separate one compound from others, and to sense the trapped molecules by electrochemical and SERS measurements.[264] By applying selected electrical signals, such as potential or current scans or pulses, these molecules could be released to the environment in an easy and controlled way.[265,266]

6. The chemistry of alkanethiolate SAMs

6.1 The chemistry of the S–Au bond

We will now discuss the relevance of some recent findings concerning the identification of the precise composition of thiolate-protected gold clusters, as well as the importance of the atomic structure of the interface of the gold core and the gold thiolate shell in relation to the structure of the interface for SAMs on Au(111).[120]

First, we will review experimental data regarding the chemistry of the interface, starting with the nature of the bound S atoms. XPS has been widely used to obtain information of the surface chemistry of SAMs on metal surfaces. As mentioned in Section 1, some damage to SAMs resulting from XPS measurements is possible. In the case of alkanethiolate SAMs, both the alkyl chains and the S–metal interface can be affected through dissociation of C–H, C–C, C–S and substrate–thiolate bonds produced by the emitted electrons. Thus the induced damage in alkanethiol monolayers has to be carefully considered when using XPS. Taking in mind these considerations, XPS is still a powerful tool to explore the nature of the S–Au bond and the presence of different S-containing species present at SAMs. In particular, XPS can give information on both physisorbed and chemisorbed species.

6.1.1 The S atoms. Valuable information about the chemical state of S atoms in the SAMs can be obtained from XPS measurements, and a correct assignment of the S 2p components in a XPS spectrum is a key point for SAM analysis. Essentially, the S 2p core level peak of alkanethiol SAMs on a variety of metals can be decomposed into different components (Fig. 16a), each being fitted by a doublet peak with a branching ratio of 0.5 and a spin–orbit splitting of 1.18 eV. In the case of alkanethiols on Au(111), it is possible to find up to three components, with average binding energy (BE) values of 161 (C1), 162 (C2), and 163–164 (C3) eV. In some cases other components at higher binding energies can be observed, which correspond to oxidized S species (see section 6.3).

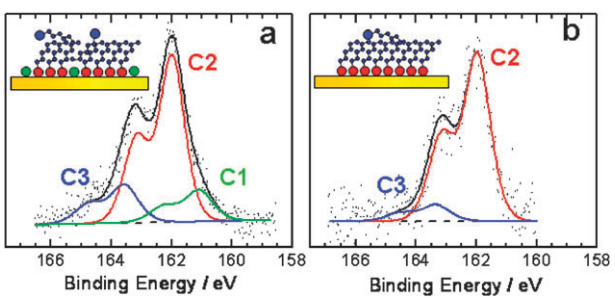

Fig. 16 S 2p XPS spectra for the standing up phases on Au(111) obtained after a 24 h incubation in a 50 μM ethanolic solution. (a) propanethiolate SAM. C1: atomic sulfur (green), C2: thiolate (red), C3: physisorbed molecules (free SH) (blue). Inset: SAM with thiolates, S and free thiols. (b) "Better quality" butanethiolate SAM showing the predominant C2 (red) component and only a small amount of C3 (blue). Inset: thiolate SAM with a small amount of free thiol.

C2 (162 eV) is usually the main component and corresponds to S chemisorbed on the gold surface through a thiolate bond.[4,5] A well-resolved peak with this single component is indicative of a high quality SAM on a metal surface (Fig. 16b). Component C1 (161 eV), not always present on the surface, has been assigned to dilute atomic S associated with some degradation of the layer or with S coming from impurities present in the thiols.[52,267] It has been shown that soft X-ray irradiation[268] and annealing of the SAMs[167] result in a clear enhancement of this component, possibly because of C–S bond cleavage.

Finally, component C3 (163–164 eV) has been assigned to free or unbound thiol. This component is significantly increased when the sample has not been well rinsed with the solvent before its introduction in the UHV chamber (Fig. 16a).[269] On the other hand, this peak can also be assigned to disulfide species.[269] As mentioned before, other oxidized sulfur species (like sulfonates or sulfates) give contributions at BE of 166 eV or higher (see Fig. 20).[270,271]

For gold nanoparticles with Au cores smaller than 5 nm, a great number of atoms are located at the nanoparticle surface. The number of surface atoms and the curvature decrease sharply as the nanoparticle size increases, reaching bulk properties for sizes larger than 10 nm. A large number of Au surface atoms are located at corners and edges of the nanoparticles: for particles 1–2 nm in size 45% of all surface atoms are located at these defective sites.[272–275] The greater concentration of atoms at surface defects and the high radius of curvature of the cluster allow a larger proportion of the Au atoms to be on the cluster surface, which in turn results in a greater coverage of the thiol monolayer on the surface.[214,276,277] EXAFS data suggest that NP smaller than 5 nm have almost twice S (θ = 2/3) as found on planar surfaces (θ = 1/3).[276,277] As already discussed,[2] this high coverage has been attributed to the occupancy of alternative binding sites (edges and corners) and can be modeled both by simple geometric[18,278–280] and computational models. A large amount of unbound molecules has been observed by XANES on gold nanoparticles covered by long alkanethiols.[276] Actually, a consequence of the high curvature radius is a decrease in the chain density as one moves away from the nanoparticle surface. The open outer structure enhances interdigitation with chains of free thiols, as mentioned in section 5.2.

In the case of dithiols in a lying down configuration only the thiolate component C2 is observed (Fig. 17a), that is, all S atoms are chemisorbed on the Au surface. On the other hand, for the standing up phase the typical S 2p signal involves not only the thiolate component C2 but also a strong signal at 163 eV (C3) arising from the free terminal SH group (Fig. 17b). For a clean dithiolate SAM on Au(111) in a

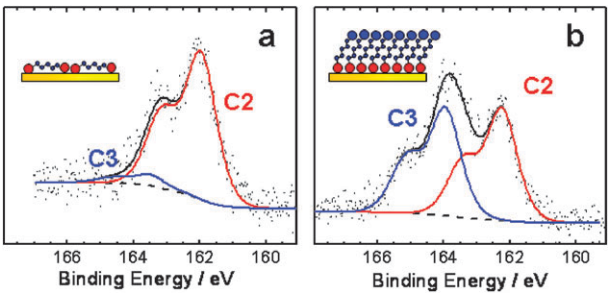

Fig. 17 S 2p XPS spectra of alkanedithiol SAMs on Au(111) prepared by immersion in 50 μM ethanolic solution for 24 h. C2 (red): thiolate; C3 (blue): free SH-terminal group. (a) Butanedithiol SAM: most of the dithiol molecules are in the lying down configuration. (b) Nonanedithiol SAM: molecules are in standing up configuration. The insets show (a) dithiols in lying down configuration, (b) dithiols in standing-up configuration.

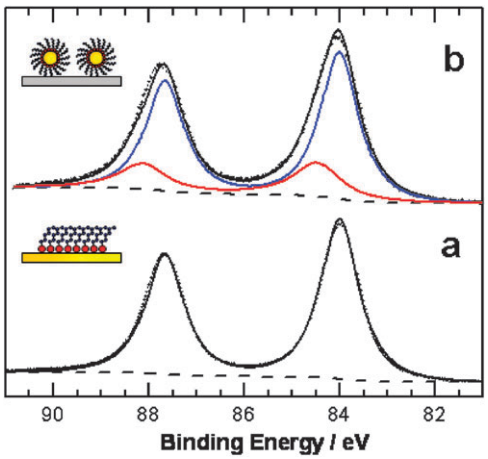

Fig. 18 XPS 4f core level for: (a) Dodecanethiolate SAM on Au(111). Only one component is needed for the fit. (b) Butanethiolate SAM on gold nanoparticles 3 nm in size supported on graphite. Blue and red lines indicate the two components needed to fit the spectrum.

standing up configuration, a C3/C2 intensity ratio equal to 1 is expected (after correction for the different attenuation of the two types of S atoms), as there is one thiolate per free SH group. This ratio is an indication of the presence of a dense standing up dithiol SAM on Au(111), free of additional physisorbed molecules or disulfide formation. On the other hand, the absence of the C3 (163 eV) component indicates the presence of all dithiols in a lying down configuration. Intermediate situations, with C3/C2 intensity ratios lower than 1, indicate that mixed domains of lying down and standing up phases coexist. On the other hand, C3/C2 ratios higher than 1 can be taken as an indication of disulfide formation in multilayers.[245]

6.1.2 The Au surface. For clean Au(111), high resolution XPS (HRXPS) spectra exhibit two components (83.93 eV and 83.62 eV)[281] that can be assigned to gold atoms in the bulk, and in the topmost surface layer, respectively. On the other hand, oxidized gold species show significant shifts in the 4f signal with respect the value of the metal: 84.3 eV[282] for thiolate–Au(I) complexes and 86 eV[283] for Au(III) species (like those found on Au_2O_3 oxides). In principle, if thiolate–Au complexes were present in the SAM (Fig. 9), one would expect some evidence of gold oxidation. In contrast, upon thiol adsorption, the HRXPS data of the 4f level for Au(111) can be fitted with a single component at ~84 eV (Fig. 18a).[281,282]

In this context, it is interesting to analyze the charge transfer between the Au and S atoms upon thiol adsorption under the light of the different models shown in Fig. 9.

Bader analysis is a robust and fast method that is used to analyze the charge of individual atoms in molecules or in condensed phase systems.[284] This algorithm decomposes the electronic charge density into individual atomic contributions.[285] Table 2 shows that, irrespective of the model, the observed charge transfer is small, resulting in a slightly positive charge on the Au atom/adatoms and a slightly negative charge on the S atom. Moreover, the charge transfer is similar to that expected for a RS–Au complex.

The change in work function upon methanethiol (MT) chemisorption (with respect to the clean, unreconstructed Au(111) surface) calculated by DFT is shown in Table 2 for the models depicted in Fig. 9. Irrespective of the surface structure, thiol adsorption results in a marked decrease in the work function. From the ΔW data the change of the surface dipole per molecule can be estimated as $\Delta d = \frac{\varepsilon_0 A \Delta W}{e}$, where A is the surface area per adsorbed methanethiolate molecule, ε_0 is the permittivity of the vacuum and e the elemental charge. Δd corresponds to the component of the dipole moment along the surface normal, and contains contributions from the charge reordering at the interface due to chemisorption, as well as from the dipole moments of the individual molecules (Table 2). The values of ΔW shown in Table 2 can be compared with the changes experimentally observed after chemisorption by using the Kelvin probe technique[286] and from photoemission measurements.[287] The latter yield ΔW values in the range −1.0 to −1.4 eV, for thiols ranging from CH_3SH to $C_{16}H_{33}SH$.[288] The Kelvin probe technique gives smaller values: for instance, a ΔW of −0.8 eV has been reported for $C_{16}H_{33}SH$.[288] It is evident that all models predict a marked lowering of the work function in the range of that experimentally observed in photoemission measurements.

On the other hand, DFT calculations for thiol adsorption on different sites of the unreconstructed Au(111) surface[289] show that Δd is mainly determined by the Au–S bond, while both the dipole moment of an alkanethiolate molecule and the orientation of the molecule in the SAM do not vary strongly with the size of the alkyl tail. Note that Δd is very close to d_{MT} = −0.88 D, the dipolar moment of the methanethiolate molecule. This means that the charge reordering in the S–Au bond does not produce significant changes in the dipolar moment, *i.e.* the Au–S bond is practically non-polar.

Thus, both Bader charges and calculated dipolar moments indicate that the Au–S bond is mainly covalent, with only a slightly positive charge on the Au atoms and a slightly negative charge in the S atom, similar to that found for thiolate–Au complexes. Note that the negative charge in the S atom is consistent with the XPS data for the S 2p level, for which "reduced" sulfur is observed. The question now is to

give a plausible explanation for the lack of shift observed in the Au 4f core level, considering that the oxidized state is similar to that found in thiolate–Au complexes, for which a shift in about 0.3 eV has been reported.[282] One possible explanation would be the contribution of bulk gold, which could completely mask the signal arising from the small population of oxidized Au atoms/adatoms.[282]

The effect of the bulk Au contribution could be minimized by using thiol-protected Au nanoparticles, because they exhibit large surface-to-volume ratios. For relatively large thiol-capped nanoparticles no negative Au $4f_{7/2}$ BE shift has been observed, as reported for planar Au surfaces.[282] It has been stated that this effect could arise from a combination of the surface atoms having a shift to lower BE (up to −0.4 eV); and the oxidized state of the gold causing a counteracting shift to a higher BE (up to +0.3 eV). The net effect could be a fortuitous positioning of the Au $4f_{7/2}$ XPS peak at, or near, the shift of bulk Au(0).

A series of *n*-dodecanethiol-capped Au nanoparticles prepared by colloidal synthesis techniques in the presence of the thiol has been investigated by XANES and XPS.[290] The experimental results only show a small 4f shift of +0.36 eV for the smallest nanoparticles (1.6 nm diameter). It was concluded that a strong covalent interaction involved some charge transfer from the nanoparticle to the thiol, in agreement with electronegativity considerations. However, this interpretation was soon questioned in terms of the so-called final state effects.[291] In fact, it was argued that a strong Coulomb interaction between the core hole and the outgoing photoelectron would produce a significant BE shift toward higher energies that should be considered when interpreting the photoemission spectra of nanoparticles.

At the same time a detailed line-shape analysis of the Au 4f core level photoemission spectra from high-resolution synchrotron-based measurements on 3 nm dodecanethiolate-passivated Au nanoparticles[292] showed two components shifted to higher BE with respect to the peaks for clean gold and for alkanethiolate SAMs on planar substrates. These two components were related to the inner Au atoms (lower BE) and surface Au atoms bound to surface dodecanethiolates (higher BE). Similar results are shown in our 4f XPS spectra recorded for 3 nm sized gold nanoparticles covered by butanethiolate SAMs (Fig. 17b). The shift of the surface component was assigned to the different chemical states in the surface Au atoms bound to the thiol, *i.e.* the charge transfer occurs from the core Au nanoparticles to the surface passivants. On the other hand, the shift of the bulk component in the Au 4f core-level was associated with final state effects.[293] The important role of final state effects was supported by the marked 4f core level shift for non-capped small Au nanoparticles (less than 70 atoms), observed irrespective of the substrate onto which they were supported.[294]

Moreover, recently, it has been found that the interaction of the thiol sulfur headgroup with small Au cluster (1 nm in size) surfaces leads to a 0.41 eV positive BE shift in the Au 4f core level.[295] However, as no line width broadening could be observed in these measurements, it was concluded that the thiol–gold interaction would affect the whole particle and not only the surface, where the Au–S bond is actually located. The authors also observed changes in the valence band shape that were interpreted as re-hybridization of Au 5d electrons due to the creation of Au–S bonds.

From this discussion it is evident that thiol adsorption introduces changes in the Au surface atoms. However, the origin of the 4f core level shift in thiol-capped Au nanoparticles is still controversial.

6.2 The impact of S–Au interface on material properties

The structure and charge distribution at the Au–S interface as previously discussed could affect different properties, such as electron transport,[286] and originate interesting phenomena such as magnetism in small Au nanoparticles,[296] and surface stress on thin gold films.[297] We will briefly discuss some of these points in the following sections.

6.2.1 Magnetism. An interesting question is to explain how a ferromagnetic moment arises in thiol-capped gold nanoparticles, given the diamagnetic behaviour of bulk gold. Magnetic properties of thiol-capped gold nanoparticles have been recently reported.[296,298] and are of great interest for their applications as materials for data storage, and in health and medicine, where gold nanoparticles guided by a magnetic field could be used to kill cancer cells, for medical imaging, in hyperthermia treatments, and for drug delivery systems.[299]

The apparent ferromagnetism of 2 nm dodecanethiolate-capped Au nanoparticles has been associated with 5d localized holes generated by Au–S bonds.[296,300–303] These holes give rise to localized magnetic moments that are frozen due to the combination of the high spin–orbit coupling of gold, and the symmetry reduction associated with Au–Au and Au–S bonding. According to electron circular dichroism measurements carried out on thiolated organic monolayers on gold,[304] the magnetic moment originates from the orbital momentum. Highly anisotropic giant moments were also observed for self-organized organic molecules linked by thiols bonds to gold films.[305] This phenomenon is due to the directional nature of the assembled organic layers.[306] Straight chains with a well-defined symmetry axis can induce orbital momentum on surface electrons close to the binding atoms. The orbital momentum not only contributes to the magnetization but also to the local anisotropy, giving rise to permanent magnetism.[307] An explanation invoking strong spin–orbit interaction has also been given.[308,309] The importance of the S–Au bond in the magnetic properties has been supported by the fact that Au nanoparticles with similar size but stabilized by means of surfactants with weaker molecule–Au interactions are diamagnetic,[307] or exhibit weaker magnetic interactions.[310]

On the other hand, it has been found that the observed ferromagnetism decreases as the gold nanoparticle size decreases.[311] Size-reduction induced ferromagnetism effects have been also observed in azobenzenethiol-modified gold nanoparticles. For 1.7 nm size Au nanoparticles ferromagnetism was observed, even at room temperature, while diamagnetism was dominant for 5.0 nm size particles.[311] It has been proposed that the size dependence of magnetization in gold nanoparticles results from a delicate balance between the number of atoms in the surface and in the core.[312]

In summary, the available explanation of orbital ferromagnetism and giant magnetic anisotropy of Au at the nanoscale assumes the induction of orbital motion of surface electrons around ordered arrays of Au–S bonds.[313] However, recent theoretical calculations have shown that gold clusters are intrinsically magnetic due to the hybridization of the atomic orbitals.[312] In fact, bare octahedral clusters (without any thiol capping) are expected to be magnetic for cluster sizes of approximately 38 atoms and larger. The role of the S–Au bond in magnetic properties of gold nanoparticles thus requires more theoretical and experimental results.

6.2.2 Surface stress. It is known that the formation of the thiol and dithiol standing up phases ($\sqrt{3} \times \sqrt{3}$ R30°, c(4 × 2)) on Au(111) is accompanied by an increase in surface stress. Surface stress arises when surface atoms undergo some dynamic structural process resulting in a change in density when they are rigidly attached to a substrate. When the strength of bonds between surface atoms are stronger than those amongst bulk atoms, a tensile surface stress is produced, leading to a concave surface curvature.[314] In contrast, when surface atoms tend to repel each other, a compressive surface stress is induced, resulting in a convex surface curvature (Fig. 19).

This phenomenon can be applied to the chemical sensing of numerous target molecules by means of micro-mechanical cantilever-based sensors.[315] Since it is possible to sensitize one surface of a cantilever differently than the opposing surface, a surface stress is induced when the target molecule interacts with the sensitized surface, and the cantilever bends due to the difference in the surface stress acting on both sides of the cantilever, allowing detection.

SAMs are usually part of cantilever-based sensing devices, so that surface stress induced by thiol self-assembly can be used as a model system to shed light into the origins of the intermolecular forces involved in these phenomena. Berger *et al.*[297] have measured the surface stress associated with the formation of dense alkanethiol SAMs. They found that the induced surface stress increases during self-assembly, and that it also increases with the alkanethiol chain length. On the other hand, a clear correlation between surface stress and the morphology of the gold substrate has been found.[142] The surface stress associated with a high-quality SAM was found to be at least an order of magnitude larger than for a SAM formed on small-grained gold. SAM formation on Au surfaces with smaller grains seems to yield lying-down phases that are not able to undergo the transition to the standing-up phase. However, other recent results have indicated that alkanethiol adsorption-induced surface stress is largely unaffected by the surface roughness of the substrate.[316]

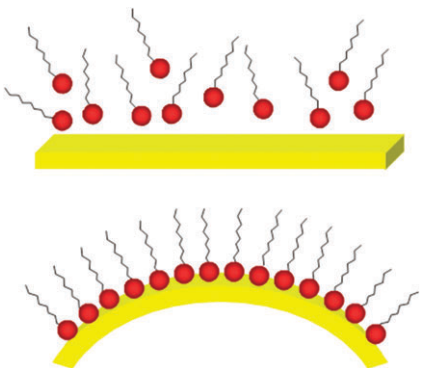

Fig. 19 Changes induced in the gold surface upon thiol adsorption. The formation of dense standing up phases leads to a compressive surface stress (not to scale).

In principle, intermolecular interactions have been considered to be the main contribution to the compressive surface stress.[317,318] However, chain–chain interactions between adjacent alkanethiol molecules forming the $\sqrt{3} \times \sqrt{3}$ R30° lattice on the Au(111) surface resulted in attractive forces (1–2 kcal mol^{-1} per methylene) that should produce a tensile rather than a compressive surface stress. Therefore, chain–chain interactions cannot be regarded as the origin of the overall induced surface stress.

The modification of the underlying gold substrate electronic structure due to thiolate adsorption has also been considered as the possible cause for the development of the surface stress.[293] A simple electrostatic repulsion model, where Au^+S^- units were treated as adjacent dipoles repelling each other, resulted in a compressive surface stress, although they only accounted for a small fraction of the overall observed surface stress.[294,297] On the other hand, changes in charge distribution of the gold surface atoms could account for the large surface stresses observed.[319] In fact, charge transfer from the gold surface atoms to the S atoms (Table 2) reduces the bond strength between gold surface atoms, increasing interatomic distances, and thus producing compressive surface stress. The charge redistribution resulting from alkanethiol adsorption could provide the necessary driving force for the creation of the observed vacancy islands (Fig. 12 and 13).[142,320]

A theoretical framework to understand the adsorption effect on the mechanical response of nanomaterials and nanodevices is still needed. Recently, the relationships between the adsorption-induced surface stress, the van der Waals and Coulomb interactions in terms of the physical and chemical interactions between adsorbates and solid surfaces has been presented.[321]

6.2.3 Electronics. Electron transport measurements through alkanethiol and alkanedithiols molecules chemisorbed on Au surfaces,[322,323] either by Scanning Tunneling Spectroscopy (STS)[324,325] or conductive-AFM,[326,327] have shown that the current decreases exponentially with the chain length with a decay factor β ranging from 0.5 to 1 A^{-1}, which indicates a low tunneling efficiency. Interestingly, the same values have been obtained both for one-side or two-side chemicontacts.[328–330] It has also been observed that the thiol or dithiol contact resistance should be very small in relation to the resistance arising from the insulating hydrocarbon chains. The low β ($\sim$0.5) and high β ($\sim$1) values[323] could reflect different transport mechanisms. It is generally accepted that the current flows following the bond overlap along the molecules (through-bond mechanism). However, a direct component from one electrode to the other across the molecules acting as a dielectric medium (through-space tunneling) can always be present. There has been experimental support for both models, making clear that more theoretical and experimental work is needed to decide which mechanism is dominant under

certain experimental conditions. To this end, a precise control of the SAM thickness is a crucial point. Therefore, the existence of domains with different tilts, for instance rectangular phases of alkanethiols ($2 \times \sqrt{3}$ or $4 \times \sqrt{3}$) (Fig. 8), lying down domains in mixed SAMs of dithiols or disorganized regions such as domain boundaries (Fig. 13b), should introduce a large scatter in the experimental data. In the metal–thiol–metal junction the top electrode will have areas of contact, or very close possible contact, with the bottom electrode, leading to cases (or situations) where other conduction mechanisms are possible.[331]

On the other hand, STM has been employed to measure single-molecule conductance by repeatedly forming molecular junctions in which dithiol molecules are covalently bound to two gold electrodes (tip and working electrode). Conductance histograms can then be constructed from the individual measurements.[332] The well-defined peaks in the histogram are located at integer multiples of a fundamental conductance value, which is used to identify the conductance of a single molecule. Several groups have performed this kinds of experiment.[332–335]

The key role of the S–Au bond in determining the electron transfer through different molecules has been discussed. For terthiophene molecules with S or Se linkages it has been found that the latter provides a better electron coupling between the Au electrode and a molecular wire.[336] It has also been observed that the contact resistance for CN/Au[337] and NH_2/Au[338,339] links are lower than for the Au/S interface. Recently, it has been shown that Au–C and Au–S tethered Os complexes show similar electron transfer mechanisms in STM "tunneling" gap configurations.[340] It has also been reported from DFT calculations that thiol-metal bonds are not good "alligator clips"; in fact, the conductance for carbenes and isocyanide linkages is nearly the same and much larger than that for thiolates.[341]

The position of the HOMO and LUMO levels is also an important question to understand electron transport through SAMs. UPS measurements have shown no evidence of molecular levels within 5 eV from the Au Fermi level.[342] It was also found that the contact resistance decreases as the substrate work function increases, suggesting that tunneling is HOMO assisted. The energy separation between the Fermi level and the closest molecular orbital (typically the HOMO) is one of the main parameters governing electronic devices.[342]

The key role of the Au/S interface in determining the level alignment has been theoretically investigated by using π-conjugated thiols with different terminal groups (NH_2, SH, CN).[343] It was found that, despite the fact that the molecules display different frontier orbital energies, the HOMO levels are pinned at a constant energy offset with respect to the metal Fermi level. This means that the local electrostatic potential at the S–Au bond lines up the HOMO at the same energy below the Fermi level, irrespective of the molecule. On the other hand, the molecular properties strongly impact the metal work function.[343] It was proposed that the relative gap between the Fermi level and the orbitals of the molecule that mediate tunneling is shifted by an amount equal to the product of the electronic charge and the surface dipole moment.[335]

From the above discussion, it is evident that a good control of surface structure, chain ordering, and a precise knowledge of the S–Au interface are needed for an understanding of the electronic properties of thiolate and dithiolate SAMs if they are to be used as active or passive elements in electronic devices.

6.3 Chemical stability: SAM degradation

The chemical stability of thiolate and dithiolate SAMs is one of the most serious problems for their applications in ambient and aqueous environments. Indeed, there are clear evidences that SAMs can degrade in ambient conditions, according to reactions:[270,344]

$$2\ \mathrm{RS{-}Au} \rightarrow \mathrm{RSSR} + 2\ \mathrm{Au} \qquad (8)$$

$$\mathrm{RS{-}Au} + \mathrm{H_2O} + \mathrm{O_3} \rightarrow \mathrm{RSO_3H} + \mathrm{HO{-}Au} \qquad (9)$$

Disulfides (reaction 8) and sulfonates (reaction 9) are not chemisorbed, and therefore, can be easily removed from the Au surface. Thus, these reactions could lead to a rapid deterioration of the thiolate SAM-based devices or SAM-modified surfaces.[344–346]

Several studies have dealt with the role of oxygen,[346] ozone, UV radiation,[347,348] hydrocarbon chain length, the nature of the end group,[349–351] the substrate structure,[352] and the environment where the reaction takes place (air, water, ethanol) in thiolate SAM degradation.[345,353] It has been reported that the degradation rate decreases as the chain length increases, while it increases with decreasing gold grain size.[271,352] Oxidation in the absence of light has also been observed. Ethanol seems to be the most aggressive environment for thiolate headgroups.[145,344,345] Disulfides have been proposed as the main final product of degradation in liquid media, and also in thermal desorption experiments (reaction 8).[354–357] In addition, sulfonate formation is expected after either air or liquid media exposure (reaction 9).[344,358] Therefore, in liquid media, the desorption rate increases because both degradation processes are possible. In contrast to the rapid degradation under ambient conditions and in liquid phase, no significant changes in the chemical structure of the S headgroup of octanethiol SAMs on Au have been observed[359] after long term storage in UHV in the absence of light.

On the other hand, there is electrochemical and spectroscopic evidence that 4-mercaptopyridine decomposes spontaneously into monomeric and oligomeric sulfur upon prolonged exposure, even in diluted solutions.[360] In contrast, no degradation was observed for 2-mercaptopyridine under the same experimental conditions.

Concerning the role of the substrate structure, it has been reported that nanostructured gold exhibits a higher resistance to thiolate degradation than Au(111) substrates.[358] Thiolate SAMs on Au(111) surfaces show a significant amount of sulfonates when exposed to ambient conditions for two weeks.[358] (Fig. 20a,c). On the other hand, for the same time exposure to ethanolic solutions (the most aggressive environment), half of the thiolates were transformed into disulfides.[361] In contrast, a negligible amount of sulfonates was observed for SAMs self-assembled on nanostructured Au in ambient conditions,[270] while no degradation occurred in pure ethanol.[361]

The increased chemical and electrochemical stability of the SAMs has been related to the presence of a larger number of substrate defects, such as gold islands, vacancies, steps and

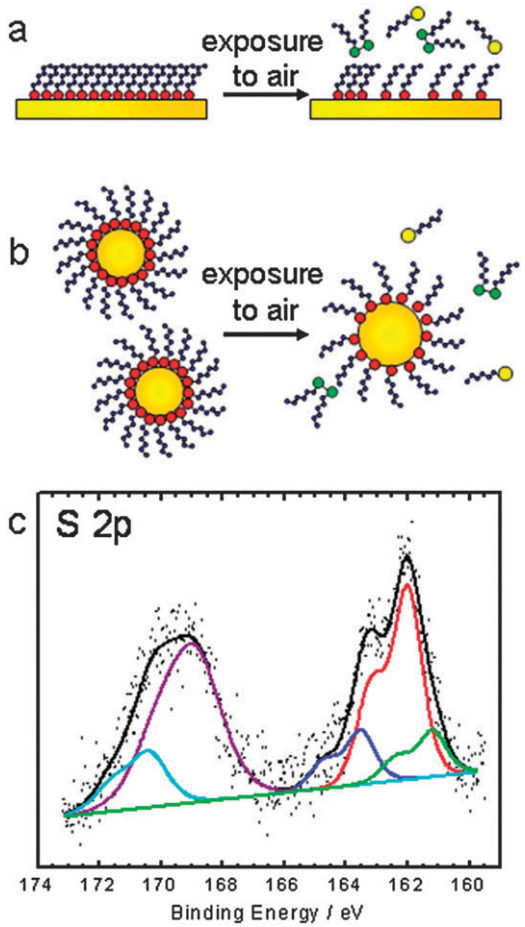

Fig. 20 Schemes showing the effect of air exposure on (a) a thiolate SAM on Au(111) and (b) thiolate-capped gold nanoparticles. Molecules with red, green and yellow S headgroups are thiolates, disulfides and sulfonates, respectively. Note the sintering of the Au NP upon thiolate oxidation. (c) S 2p XPS spectra for a nonanethiol SAM on Au(111) prepared by 24 h incubation in 50 μM ethanolic solution and exposed for 15 days to ambient conditions. The presence of oxidized sulfur species at BE greater than 166 eV (purple and cyan components) indicates the degradation of the SAM. The C1 (green), C2 (red), and C3 (blue) components are also observed.

adatoms; the adsorption energy is larger at low coordinated sites of the gold surface. Nanostructured gold is thus an attractive platform for the fabrication of different types of thiolate-based devices (of course, if the order of the hydrocarbon chains is not important). An enhanced stability of SAMs can also be expected for other defective polycrystalline Au substrates with open rough surfaces, like those prepared by sputtering or vapor deposition. The advantages of nanostructured substrates are not only related to their increased stability, but also to the fact that they are SERS active[362] and have a high signal-to-noise ratio for amperometric detection because of their high real area, which makes them useful platforms for molecular sensing devices.[363]

Thiolate-capped gold nanoparticles are known to be stable in toluene or hexane solutions for several years. However, when the solvent is evaporated and the particles are crystallized onto a substrate, the structural stability of the particles is affected (Fig. 20b). Subjecting the particles to electron beam irradiation in a TEM can be sufficient to disrupt the protective alkanethiolate cap.[364] The degradation process can take place even in ambient conditions (Fig. 20b). Degradation of the thiol-capped gold nanoparticles supported on highly oriented pyrolytic graphite has been observed after two-week exposure to ambient conditions,[270] with formation of a significant amount of oxidized S species (binding energies >166 eV). Sintering of Au nanoparticles (2–7 nm) in ambient conditions has also been observed when supported on Si_3N_4 substrates.[365] It was found that Au nanoparticles below 4 nm can spontaneously sinter in the dried out state at room temperature over extended time periods, as a consequence of thiol destabilization and their depressed melting points. This room temperature sintering phenomenon stops, however, when the particle has grown to a size of about 7 nm.

The chemical stability of the thiolate cap is a key point for gold nanoparticle based devices whose function depends on the structural integrity of the individual particles over long time periods. For this reason, the effect of the substrate, particle size, and storage conditions should be carefully investigated. Moreover, new thiol cappings with higher oxidation resistance should be developed to solve these problems.[366]

6.4 Thermal stability

The thermal stability of thiol and dithiol SAMs on gold is an important issue that has to be taken into account before considering their use for a technological application. Thermal desorption of SAMs has been studied by different groups and with different techniques, including TPD (either with mass spectrometry or He reflectivity detection).[167,357,367–370] The desorption process can be affected by different factors, such as chain length,[368] substrate temperature during adsorption,[370] and surface roughness,[136] among others.

Delamarche *et al.* reported on the effect of annealing dodecanethiol SAMs at around 373 K.[151] During the annealing process the vacancy islands (Fig. 12 and 13) typically observed in alkanethiol SAMs almost disappeared and larger molecular domains without any missing rows or domain boundaries were formed. When the annealing was continued, dodecanethiolate molecules began to desorb from the Au surface, and after 48 h they had been almost completely desorbed. This temperature (373 K) constitutes a reasonable compromise between SAM reorganization and disruption; at this temperature the speed of reorganization of the SAM is evidently faster than that of desorption and chemical reaction of the sulfur headgroups.[168] However, HREELS measurements of octadecanethiol SAMs on Au thin films obtained after annealing the sample at 375 K showed the appearance of a S–S stretching mode at 530 cm^{-1}, a direct observation of sulfur dimers.[136] The appearance of this mode only when this temperature was reached indicates that there is an energy barrier for disulfide formation which has been assigned to the formation of *gauche* defects at the S–C bonds. The first step is largely affected by the hydrocarbon chain length, so that van der Waals interactions are a key factor in governing the activation energy for desorption as disulfides.[355]

Fig. 21 shows a typical thermal desorption curve of a thiolate SAM from the Au(111) surface recorded by following

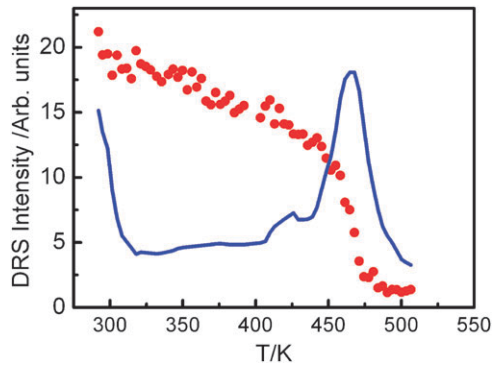

Fig. 21 Intensity for H DRS from hexanethiolate SAM on Au(111) as a function of the temperature. The sudden decrease at 450 K is related to desorption of thiolate species from the Au surface. The derivative (blue curve) shows the peak centered at 460 K. Desorption at low temperature (300 K) is assigned to desorption of physisorbed thiols. Data taken from ref. 108 with permission of the American Chemical Society.

the H intensity by TOF-DRS. The curve exhibits a sudden decrease in the H signal at ~450 K, and an almost complete thiolate desorption at ~500 K. In the same work, no S traces were observed, indicating that the S–C scission is not efficient. The derivative (Fig. 21) shows the large peak centered at 460 K, which has been assigned to thiolate desorption as disulfide species (see reaction (8)) from the dense standing up phases (Fig. 7).[355,371] In these phases the small 0.5 nm distance facilitates dimerization between adjacent molecules. In some cases, though, a second peak at 500–550 K has been reported[368] which has been related to desorption of thiolates as monomers from the more diluted striped phases (Fig. 6).[354,355] However, Ito *et al.*[350] have investigated the desorption process of structural isomers of propanethiols. For *n*-propanethiol SAM desorption they reported two peaks at 375 K and 450 K that were assigned to disulfide and thiolate desorption, respectively. Disulfide formation was hindered for propanethiolate isomers that formed lattices with larger S–S distances.[345] The desorption of monomers was also affected by the hydrocarbon chains, the desorption temperature following the molecular density. The authors concluded that there was no obvious correlation between steric hindrance of the molecules and the desorption behaviour. This is an interesting point that deserves further experimental work.

The thermal stability of alkanethiolate-capped gold nanoparticles has also been investigated. Results from XPS data have showed that short thiols (C3, C4, and C5) began to desorb from the sample at 363–413 K, whereas for long thiols (C6–C8, and C16) this threshold was around 433 K.[372] The changes in desorption temperature reflect the stabilizing forces between the thiol molecules, which increase with longer chain length. In contrast to chemical degradation, the thermal stability was independent of the Au nanoparticle size.

Several strategies have been used to improve the thermal stability of SAMs on Au surfaces: modification of the gold surface with an underpotentially deposited Ag layer surface[373] (here place exchange occurs, and a thiolate SAM on silver is obtained), formation of a hydrogen bond network derived from amide groups,[374] and the use of electron-irradiated aromatic SAMs.[375] In this case intermolecular cross-links are formed, stabilizing the SAMs up to 800 K. As in the case of chemical stability, the search of new strategies to improve thermal stability is an important issue that needs further investigation.

7. Conclusions and outlook

The surface structures of thiolate SAMs on gold have been reviewed, highlighting the multiple problems and controversy that still exists in different topics of what is often considered as a simple surface science model system. We have focused on some hot points that require further investigation: the chemistry and structure of the S headgroup–Au interface, SAM quality (structural defects and chain order), and chemical and thermal stability for planar, rough, and nanocurved surfaces. A better knowledge of basic aspects of these points will have not only a strong impact in the wide field of SAM applications, but also in our understanding of the gold chemistry in two dimensions.

Acknowledgements

We acknowledge financial support from ANPCyT (PICT 06-621, PICT 05-32439, PICT-CNPQ 08-019) and CONICET (PIP 112-200801-00362) (Argentina), and MCI (CTQ2008-06017/BQU) (Spain). RCS is a Guggenheim Foundation Fellow. MEV is a member of the research career of CIC. Authors thank G. Andreasen and F. Terán Arce for taking some of the STM images shown.

References

1 J. L. Wilbur and G. M. Whitesides, in *Nanotechnology*, ed. G. Timp, Springer Verlag, New York, 1999.
2 J. C. Love, L. A. Estroff, J. K. Kriebel, R. G. Nuzzo and G. M. Whitesides, *Chem. Rev.*, 2005, **105**, 1103–1169.
3 B. D. Gates, Q. Xu, M. Stewart, D. Ryan, C. G. Willson and G. M. Whitesides, *Chem. Rev.*, 2005, **105**, 1171–1196.
4 L. H. Dubois and R. G. Nuzzo, *Annu. Rev. Phys. Chem.*, 1992, **43**, 437–463.
5 P. Somasundaran, B. Markovic, X. Yu and S. Krishnakumar, in *Handbook of Surface and Colloid Chemistry*, ed. K. S. Birdi, CRC Press, Boca Ratón, 2002, pp. 387–435.
6 E. Ruckenstein and Z. F. Li, *Adv. Colloid Interface Sci.*, 2005, **113**, 43–63.
7 D. D. Gandhi, M. Lane, Y. Zhou, A. P. Singh, S. Nayak, U. Tisch, M. Eizenberg and G. Ramanath, *Nature*, 2007, **447**, 299–302.
8 Y. Cai, *Langmuir*, 2009, **25**, 5594–5601.
9 A. R. Morrill, D. T. Duong, S. J. Lee and M. Moskovits, *Chem. Phys. Lett.*, 2009, **473**, 116–119.
10 A. Ulman, Academic Press, Boston, 1991.
11 A. Heijink, J. Schwartz, M. E. Zobitz, K. Nicole Crowder, G. E. Lutz and J. D. Sibonga, *Clin. Orthop. Relat. Res.*, 2008, **466**, 977–984.
12 B. M. Silverman, K. A. Wieghaus and J. Schwartz, *Langmuir*, 2005, **21**, 225–228.
13 S. Pawsey, K. Yach and L. Reven, *Langmuir*, 2002, **18**, 5205–5212.
14 E. L. Hanson, J. Schwartz, B. Nickel, N. Koch and M. F. Danisman, *J. Am. Chem. Soc.*, 2003, **125**, 16074–16080.
15 E. Hoque, J. A. DeRose, P. Hoffmann, H. J. Mathieu, B. Bhushan and M. Cichomski, *J. Chem. Phys.*, 2006, **124**, 174710–174716.
16 E. Hoque, J. A. DeRose, B. Bhushan and K. W. Hipps, *Ultramicroscopy*, 2009, **109**, 1015–1022.
17 J. Amalric, P. H. Mutin, G. Guerrero, A. Ponche, A. Sotto and J.-P. Lavigne, *J. Mater. Chem.*, 2009, **19**, 141–149.
18 R. H. Terrill, T. A. Postlethwaite, C. H. Chen, C. D. Poon, A. Terzis, A. Chen, J. E. Hutchison, M. R. Clark, G. Wignall,

J. D. Londono, R. Superfine, M. Falvo, C. S. Johnson Jr, E. T. Samulski and R. W. Murray, *J. Am. Chem. Soc.*, 1995, **117**, 12537–12548.
19 B. R. Martin, D. J. Dermody, B. D. Reiss, M. Fang, L. A. Lyon, M. J. Natan and T. E. Mallouk, *Adv. Mater.*, 1999, **11**, 1021–1025.
20 O. Azzaroni, P. L. Schilardi and R. C. Salvarezza, in *Encyclopedia of Nanoscience and Nanotechnology*, ed. H. S. Nalwa, American Scientific Publishers, 2004, vol. 5, p. 835.
21 O. Azzaroni, M. H. Fonticelli, G. Benitez, P. L. Schilardi, R. Gago, I. Caretti, L. Vázquez and R. C. Salvarezza, *Adv. Mater.*, 2004, **16**, 405–409.
22 J. Sagiv, *J. Am. Chem. Soc.*, 1980, **102**, 92–98.
23 U. Drechsler, B. Erdogan and V. M. Rotello, *Chem.–Eur. J.*, 2004, **10**, 5570–5579.
24 M. C. Daniel and D. Astruc, *Chem. Rev.*, 2004, **104**, 293–346.
25 O. Azzaroni, M. Cipollone, M. E. Vela and R. C. Salvarezza, *Langmuir*, 2001, **17**, 1483–1487.
26 G. Brunoro, A. Frignani, A. Colledan and C. Chiavari, *Corros. Sci.*, 2003, **45**, 2219–2231.
27 C. M. Whelan, M. Kinsella, L. Carbonell, H. Hong Meng and K. Maex, *Microelectron. Eng.*, 2003, **70**, 551–557.
28 *N. a. Nanomechanics*, ed. B. Bhushan, Springer, Berlin-Heidelberg, 2008.
29 R. Maboudian, W. R. Ashurst and C. Carraro, *Sens. Actuators, A*, 2000, **82**, 219–223.
30 Y. Wang, Y. Zhou, J. Sokolov, B. Rigas, K. Levon and M. Rafailovich, *Biosens. Bioelectron.*, 2008, **24**, 162–166.
31 H. Chen, C. K. Heng, P. D. Puiu, X. D. Zhou, A. C. Lee, T. M. Lim and S. N. Tan, *Anal. Chim. Acta*, 2005, **554**, 52–59.
32 T. J. Huang, B. Brough, C.-M. Ho, Y. Liu, A. H. Flood, P. A. Bonvallet, H.-R. Tseng, J. F. Stoddart, M. Baller and S. Magonov, *Appl. Phys. Lett.*, 2004, **85**, 5391–5393.
33 L. Venkataraman, J. E. Klare, I. W. Tam, C. Nuckolls, M. S. Hybertsen and M. L. Steigerwald, *Nano Lett.*, 2006, **6**, 458–462.
34 John A. Rogers and Rogers G. Nuzzo, in *Mater. Today*, 2005, vol. 8, pp. 50–56,.
35 X. Jiang, D. A. Bruzewicz, A. P. Wong, M. Piel and G. M. Whitesides, *Proc. Natl. Acad. Sci. U. S. A.*, 2005, **102**, 975–978.
36 S. Takeuchi, W. R. DiLuzio, D. B. Weibel and G. M. Whitesides, *Nano Lett.*, 2005, **5**, 1819–1823.
37 D. G. Castner and M. Ratner, in *Frontiers in Surface Science*, ed. C. B. Duke and E. W. Plummer, North Holland, Amsterdam, 2002.
38 Scientific American, vol 285 Issue 3 (2001), Science: Supramolecular Chemistry and Self Assembly vol. 295 pp. 2313–2556 (2002).
39 L. A. Bumm, J. J. Arnold, M. T. Cygan, T. D. Dunbar, T. P. Burgin, L. Jones, II, D. L. Allara, J. M. Tour and P. S. Weiss, *Science*, 1996, **271**, 1705–1707.
40 J. M. Tour, *Acc. Chem. Res.*, 2000, **33**, 791–804.
41 T. Sugawara and M. M. Matsushita, *J. Mater. Chem.*, 2009, **19**, 1738–1753.
42 A. Lio, D. H. Charych and M. Salmeron, *J. Phys. Chem. B*, 1997, **101**, 3800–3805.
43 R. Levicky, T. M. Herne, M. J. Tarlov and S. K. Satija, *J. Am. Chem. Soc.*, 1998, **120**, 9787–9792.
44 B. Bonanni, A. R. Bizzarri and S. Cannistraro, *J. Phys. Chem. B*, 2006, **110**, 14574–14580.
45 E. T. Castellana and P. S. Cremer, *Surf. Sci. Rep.*, 2006, **61**, 429–444.
46 M. Brust, M. Walker, D. Bethell, D. J. Schiffrin and R. Whyman, *J. Chem. Soc., Chem. Commun.*, 1994, 801–802.
47 T. Shimizu, T. Teranishi, S. Hasegawa and M. Miyake, *J. Phys. Chem. B*, 2003, **107**, 2719–2724.
48 G. F. Paciotti, L. Myer, D. Weinreich, D. Goia, N. Pavel, R. E. McLaughlin and L. Tamarkin, *Drug Delivery*, 2004, **11**, 169.
49 K. J. C. van Bommel, A. Friggeri, D. Mateman, F. A. J. Geurts, K. G. C. van Leerdam, W. Verboom, F. C. J. M. van Veggel and D. N. Reinhoudt, *Adv. Funct. Mater.*, 2001, **11**, 140–146.
50 R. Haag, M. A. Rampi, R. E. Holmlin and G. M. Whitesides, *J. Am. Chem. Soc.*, 1999, **121**, 7895–7906.
51 Y.-J. Han and J. Aizenberg, *Angew. Chem., Int. Ed.*, 2003, **42**, 3668–3670.
52 C. Vericat, M. E. Vela, G. A. Benitez, J. A. Martin Gago, X. Torrelles and R. C. Salvarezza, *J. Phys.: Condens. Matter*, 2006, **18**, R867–R900.
53 P. Fenter, A. Eberhardt and P. Eisenberger, *Science*, 1994, **266**, 1216–1218.
54 M. G. Samant, C. A. Brown and J. G. Gordon II, *Langmuir*, 1991, **7**, 437–439.
55 K. Heister, D. L. Allara, K. Bahnck, S. Frey, M. Zharnikov and M. Grunze, *Langmuir*, 1999, **15**, 5440–5443.
56 C. M. Whelan, C. J. Barnes, C. G. H. Walker and N. M. D. Brown, *Surf. Sci.*, 1999, **425**, 195–211.
57 T. M. Schultz, *PhD Thesis*, Aarhus University, DK, 1998.
58 W. Azzam, P. Cyganik, G. Witte, M. Buck and C. Wöll, *Langmuir*, 2003, **19**, 8262–8270.
59 R. Gerlach, G. Polanski and H. G. Rubahn, *Thin Solid Films*, 1998, **318**, 270–272.
60 N. Camillone III, T. Y. B. Leung, P. Schwartz, P. Eisenberger and G. Scoles, *Langmuir*, 1996, **12**, 2737–2746.
61 P. A. Lewis, Z. J. Donhauser, B. A. Mantooth, R. K. Smith, L. A. Bumm, K. F. Kelly and P. S. Weiss, *Nanotechnology*, 2001, **12**, 231–237.
62 O. Cavalleri, A. Hirstein, J.-P. Bucher and K. Kern, *Thin Solid Films*, 1996, **284–285**, 392–395.
63 D. E. Weisshaar, B. D. Lamp and M. D. Porter, *J. Am. Chem. Soc.*, 1992, **114**, 5860–5862.
64 T. Sumi and K. Uosaki, *J. Phys. Chem. B*, 2004, **108**, 6422–6428.
65 Y. Tai, A. Shaporenko, W. Eck, M. Grunze and M. Zharnikov, *Langmuir*, 2004, **20**, 7166–7170.
66 Y. Tai, A. Shaporenko, H. T. Rong, M. Buck, W. Eck, M. Grunze and M. Zharnikov, *J. Phys. Chem. B*, 2004, **108**, 16806–16810.
67 A. S. Duwez, *J. Electron Spectrosc. Relat. Phenom.*, 2004, **134**, 97–138.
68 P. Feulner, T. Niedermayer, K. Eberle, R. Schneider, D. Menzel, A. Baumer, E. Schmich, A. Shaporenko, Y. Tai and M. Zharnikov, *Surf. Sci.*, 2005, **593**, 252–255.
69 D. R. Baer, M. H. Engelhard and A. S. Lea, *Surf. Sci. Spectra*, 2003, **10**, 47.
70 F. Schreiber, *Prog. Surf. Sci.*, 2000, **65**, 151–256.
71 H. O. Finklea, *Electroanal. Chem.*, 1996, **19**, 109–335.
72 H. O. Finklea, in *Encyclopedia of Analytical Chemistry: Applications Theory and Instrumentation*, ed. R. A. Meyers, Wiley & Sons, New York, 2000.
73 D. P. Woodruff and T. A. Delchar, Cambridge University Press, Cambridge, 1994.
74 *Computational Physics*, ed. J. M. Thijssen, Cambridge University Press, Cambridge, 1999.
75 *Quantum Chemistry Approaches To Chemisorption And Heterogeneous Catalysis*, Kluwer Academic, Dordrecht, 1992.
76 J. M. Haile, *Molecular Dynamics Simulation, Elementary Methods*, Wiley, Chichester, 1992.
77 J. W. Ciszek and J. M. Tour, *Chem. Mater.*, 2005, **17**, 5684–5690.
78 A. L. Harris, L. Rothberg, L. H. Dubois, N. J. Levinos and L. Dhar, *Phys. Rev. Lett.*, 1990, **64**, 2086–2089.
79 R. Heinz and J. P. Rabe, *Langmuir*, 1995, **11**, 506–511.
80 A. Nemetz, T. Fischer, A. Ulman and W. Knoll, *J. Chem. Phys.*, 1993, **98**, 5912–5919.
81 A. Dhirani, M. A. Hines, A. J. Fisher, O. Ismail and P. Guyot-Sionnest, *Langmuir*, 1995, **11**, 2609–2614.
82 P. Fenter, P. Eisenberger, J. Li, N. Camillone, S. Bernasek, G. Scoles, T. A. Ramanarayanan and K. S. Liang, *Langmuir*, 1991, **7**, 2013–2016.
83 G. D. Aloisi, M. Cavallini, M. Innocenti, M. L. Foresti, G. Pezzatini and R. Guidelli, *J. Phys. Chem. B*, 1997, **101**, 4774–4780.
84 M. Yu, S. M. Driver and D. P. Woodruff, *Langmuir*, 2005, **21**, 7285–7291.
85 H. Rieley, G. K. Kendall, R. G. Jones and D. P. Woodruff, *Langmuir*, 1999, **15**, 8856–8866.
86 M. Fonticelli, O. Azzaroni, G. Benitez, M. E. Martins, P. Carro and R. C. Salvarezza, *J. Phys. Chem. B*, 2004, **108**, 1898–1905.
87 D. Torres, P. Carro, R. C. Salvarezza and F. Illas, *Phys. Rev. Lett.*, 2006, **97**, 226103.
88 O. Azzaroni, M. E. Vela, M. Fonticelli, G. Benítez, P. Carro, B. Blum and R. C. Salvarezza, *J. Phys. Chem. B*, 2003, **107**, 13446–13454.
89 A. Imanishi, K. Isawa, F. Matsui, T. Tsuduki, T. Yokoyama, H. Kondoh, Y. Kitajima and T. Ohta, *Surf. Sci.*, 1998, **407**, 282–292.

90 H. Rieley, G. K. Kendall, A. Chan, R. G. Jones, J. Lüdecke, D. P. Woodruff and B. C. C. Cowie, *Surf. Sci.*, 1997, **392**, 143–152.
91 J. C. Love, D. B. Wolfe, R. Haasch, M. L. Chabinyc, K. E. Paul, G. M. Whitesides and R. G. Nuzzo, *J. Am. Chem. Soc.*, 2003, **125**, 2597–2609.
92 A. Carvalho, M. Geissler, H. Schmid, B. Michel and E. Delamarche, *Langmuir*, 2002, **18**, 2406–2412.
93 H. Murayama, N. Ichikuni, Y. Negishi, T. Nagata and T. Tsukuda, *Chem. Phys. Lett.*, 2003, **376**, 26–32.
94 C. Majumder, *Langmuir*, 2008, **24**, 10838–10842.
95 J. A. Williams and C. B. Gorman, *J. Phys. Chem. C*, 2007, **111**, 12804–12810.
96 G. Corthey, A. A. Rubert, G. A. Benitez, M. H. Fonticelli and R. C. Salvarezza, *J. Phys. Chem. C*, 2009, **113**, 6735–6742.
97 Z. Mekhalif, J. Riga, J. J. Pireaux and J. Delhalle, *Langmuir*, 1997, **13**, 2285–2290.
98 S. Noêl, F. Houzé, L. Boyer, Z. Mekhalif, J. Delhalle and R. Caudano, *IEEE Trans. Compon. Packag. Technol.*, 1999, **22**, 79–84.
99 M. E. Castro and J. M. White, *Surf. Sci.*, 1991, **257**, 22–32.
100 D. R. Mullins, T. Tang, X. Chen, V. Shneerson, D. K. Saldin and W. T. Tysoe, *Surf. Sci.*, 1997, **372**, 193–201.
101 C. J. Fisher, D. P. Woodruff, R. G. Jones, B. C. C. Cowie and V. Formoso, *Surf. Sci.*, 2002, **496**, 73–86.
102 Z. Mekhalif, F. Laffineur, N. Couturier and J. Delhalle, *Langmuir*, 2003, **19**, 637–645.
103 S. Bengió, M. Fonticelli, G. Benítez, A. H. Creus, P. Carro, H. Ascolani, G. Zampieri, B. Blum and R. C. Salvarezza, *J. Phys. Chem. B*, 2005, **109**, 23450–23460.
104 M. Rohwerder and M. Stratmann, *MRS Bull.*, 1999, **24**, 43–47.
105 C. Pirlot, J. Delhalle, J. J. Pireaux and Z. Mekhalif, *Surf. Coat. Technol.*, 2001, **138**, 166–172.
106 C. L. McGuiness, A. Shaporenko, C. K. Mars, S. Uppili, M. Zharnikov and D. L. Allara, *J. Am. Chem. Soc.*, 2006, **128**, 5231–5243.
107 D. Zerulla and T. Chasse, *Langmuir*, 2002, **18**, 5392–5399.
108 L. M. Rodriguez, J. E. Gayone, E. A. Sanchez, O. Grizzi, B. Blum, R. C. Salvarezza, L. Xi and W. M. Lau, *J. Am. Chem. Soc.*, 2007, **129**, 7807–7813.
109 H. Lim, C. Carraro, R. Maboudian, M. W. Pruessner and R. Ghodssi, *Langmuir*, 2004, **20**, 743–747.
110 D. Zerulla and T. Chassé, *J. Electron Spectrosc. Relat. Phenom.*, 2009, **172**, 78–87.
111 R. G. Nuzzo and D. L. Allara, *J. Am. Chem. Soc.*, 1983, **105**, 4481–4483.
112 D. L. Allara and R. G. Nuzzo, *Langmuir*, 1985, **1**, 45–52.
113 P. L. Schilardi, P. Dip, P. C. Dos Santos Claro, G. A. Benitez, M. H. Fonticelli, O. Azzaroni and R. C. Salvarezza, *Chem.–Eur. J.*, 2006, **12**, 38–49.
114 D. Burshtain and D. Mandler, *Phys. Chem. Chem. Phys.*, 2006, **8**, 158–164.
115 A. Ulman, *Chem. Rev.*, 1996, **96**, 1533–1554.
116 D. K. Schwartz, *Annu. Rev. Phys. Chem.*, 2001, **52**, 107–137.
117 G. E. Poirier, *Chem. Rev.*, 1997, **97**, 1117–1128.
118 C. Vericat, M. E. Vela and R. C. Salvarezza, *Phys. Chem. Chem. Phys.*, 2005, **7**, 3258–3268.
119 D. P. Woodruff, *Phys. Chem. Chem. Phys.*, 2008, **10**, 7211–7221.
120 M. Walter, J. Akola, O. Lopez-Acevedo, P. D. Jadzinsky, G. Calero, C. J. Ackerson, R. L. Whetten, H. Grönbeck and H. Häkkinen, *Proc. Natl. Acad. Sci. U. S. A.*, 2008, **105**, 9157–9162.
121 A. S. Duwez, L. M. Yu, J. Riga, J. J. Pireaux and J. Delhalle, *Thin Solid Films*, 1998, **327–329**, 156–160.
122 M. Schweizer, H. Hagenström and D. M. Kolb, *Surf. Sci.*, 2001, **490**, L627–L636.
123 F. Loglio, M. Schweizer and D. M. Kolb, *Langmuir*, 2003, **19**, 830–834.
124 S. Yoshimoto, T. Sawaguchi, F. Mizutani and I. Taniguchi, *Electrochem. Commun.*, 2000, **2**, 39–43.
125 M. A. Daza Millone, H. Hamoudi, L. Rodríguez, A. Rubert, G. A. Benítez, M. E. Vela, R. C. Salvarezza, J. E. Gayone, E. A. Sánchez, O. Grizzi, C. Dablemont and V. A. Esaulov, *Langmuir*, 2009, **25**, 12945–12953.
126 P. G. Lustemberg, M. L. Martiarena, A. E. Martinez and H. F. Busnengo, *Langmuir*, 2008, **24**, 3274–3279.
127 F. Schreiber, A. Eberhardt, T. Y. B. Leung, P. Schwartz, S. M. Wetterer, D. J. Lavrich, L. Berman, P. Fenter, P. Eisenberger and G. Scoles, *Phys. Rev. B*, 1998, **57**, 12476–12481.
128 S. Xu, S. J. N. Cruchon-Dupeyrat, J. C. Garno, G.-Y. Liu, G. K. Jennings, T.-H. Yong and P. E. Laibinis, *J. Chem. Phys.*, 1998, **108**, 5002–5012.
129 G. E. Poirier and E. D. Pylant, *Science*, 1996, **272**, 1145–1148.
130 R. Yamada and K. Uosaki, *Langmuir*, 1998, **14**, 855–861.
131 S. Narasimhan and D. Vanderbilt, *Phys. Rev. Lett.*, 1992, **69**, 1564–1567.
132 F. Terán Arce, M. E. Vela, R. C. Salvarezza and A. J. Arvia, *Surf. Rev. Lett.*, 1997, **4**, 637–649.
133 P. Maksymovych, D. C. Sorescu and J. J. T. Yates, *Phys. Rev. Lett.*, 2006, **97**, 146103.
134 X. Torrelles, C. Vericat, M. E. Vela, M. H. Fonticelli, M. A. D. Millone, R. Felici, T. L. Lee, J. Zegenhagen, G. Muñoz, J. A. Martín-Gago and R. C. Salvarezza, *J. Phys. Chem. B*, 2006, **110**, 5586–5594.
135 R. G. Nuzzo, B. R. Zegarski and L. H. Dubois, *J. Am. Chem. Soc.*, 1987, **109**, 733–740.
136 I. I. Rzeznicka, J. Lee, P. Maksymovych and J. T. Yates Jr, *J. Phys. Chem. B*, 2005, **109**, 15992–15996.
137 M. Hasan, D. Bethell and M. Brust, *J. Am. Chem. Soc.*, 2002, **124**, 1132–1133.
138 L. Kankate, A. Turchanin and A. GöÍlzhäuser, *Langmuir*, 2009, **25**, 10435–10438.
139 M. Kara, H. Sasabe and W. Knoll, *Thin Solid Films*, 1996, **273**, 66–69.
140 L. B. Picraux, C. D. Zangmeister and J. D. Batteas, *Langmuir*, 2006, **22**, 174–180.
141 Y.-S. Shon and T. R. Lee, *J. Phys. Chem. B*, 2000, **104**, 8182–8191.
142 M. Godin, P. J. Williams, V. Tabard-Cossa, O. Laroche, L. Y. Beaulieu, R. B. Lennox and P. Grutter, *Langmuir*, 2004, **20**, 7090–7096.
143 S. B. Darling, A. W. Rosenbaum, Y. Wang and S. J. Sibener, *Langmuir*, 2002, **18**, 7462–7468.
144 G. E. Poirier, W. P. Fitts and J. M. White, *Langmuir*, 2001, **17**, 1176–1183.
145 J. Noh and M. Hara, *RIKEN Review*, 2001, **38**, 49.
146 W. Azzam, C. Fuxen, A. Birkner, H.-T. Rong, M. Buck and C. Wöll, *Langmuir*, 2003, **19**, 4958–4968.
147 G. Heimel, L. Romaner, E. Zojer and J.-L. Bredas, *Acc. Chem. Res.*, 2008, **41**, 721–729.
148 R. Staub, M. Toerker, T. Fritz, T. Schmitz-Hubsch, F. Sellam and K. Leo, *Langmuir*, 1998, **14**, 6693–6698.
149 T. B. Creczynski-Pasa, M. A. Daza Millone, M. L. Munford, V. R. de Lima, T. O. Vieira, G. A. Benitez, A. A. Pasa, R. C. Salvarezza and M. E. Vela, *Phys. Chem. Chem. Phys.*, 2009, **11**, 1077–1084.
150 T. Y. B. Leung, M. C. Gerstenberg, D. J. Lavrich, G. Scoles, F. Schreiber and G. E. Poirier, *Langmuir*, 2000, **16**, 549–561.
151 E. Delamarche, B. Michel, H. A. Biebuyck and C. Gerber, *Adv. Mater.*, 1996, **8**, 719–729.
152 L. Strong and G. M. Whitesides, *Langmuir*, 1988, **4**, 546–558.
153 C. E. D. Chidsey and D. N. Loiacono, *Langmuir*, 1990, **6**, 682–691.
154 C. E. D. Chidsey, G.-Y. Liu, P. Rowntree and G. Scoles, *J. Chem. Phys.*, 1989, **91**, 4421–4423.
155 L. H. Dubois, B. R. Zegarski and R. G. Nuzzo, *J. Chem. Phys.*, 1993, **98**, 678–688.
156 M. G. Samant, C. A. Brown and J. G. Gordon, *Langmuir*, 1991, **7**, 437–439.
157 C. A. Widrig, C. A. Alves and M. D. Porter, *J. Am. Chem. Soc.*, 1991, **113**, 2805–2810.
158 P. Fenter, P. Eisenberger and K. S. Liang, *Phys. Rev. Lett.*, 1993, **70**, 2447–2450.
159 N. Camillone III, C. E. D. Chidsey, G. Y. Liu and G. Scoles, *J. Chem. Phys.*, 1993, **98**, 3503–3511.
160 C. Zeng, B. Li, B. Wang, H. Wang, K. Wang, J. Yang, J. G. Hou and Q. Zhu, *J. Chem. Phys.*, 2002, **117**, 851–856.
161 B. Li, C. Zeng, Q. Li, B. Wang, L. Yuan, H. Wang, J. Yang, J. G. Hou and Q. Zhu, *J. Phys. Chem. B*, 2003, **107**, 972–984.

162 P. Paredes Olivera and M. Patrito, *FyQS I Meeting*, Bariloche, Argentina, 2004.
163 A. Riposan and G.-y. Liu, *J. Phys. Chem. B*, 2006, **110**, 23926–23937.
164 O. Azzaroni, M. E. Vela, H. Martin, A. Hernández Creus, G. Andreasen and R. C. Salvarezza, *Langmuir*, 2001, **17**, 6647–6654.
165 E. J. Calvo, M. S. Rothacher, C. Bonazzola, I. R. Wheeldon, R. C. Salvarezza, M. E. Vela and G. Benitez, *Langmuir*, 2005, **21**, 7907–7911.
166 R. G. Nuzzo, E. M. Korenic and L. H. Dubois, *J. Chem. Phys.*, 1990, **93**, 767–773.
167 E. Delamarche, B. Michel, H. Kang and C. Gerber, *Langmuir*, 1994, **10**, 4103–4108.
168 E. Delamarche, B. Michel, H. A. Biebuyck and C. Gerber, *Adv. Mater.*, 1996, **8**, 719–729.
169 J. T. Banks, T. T. Yu and H. Z. Yu, *J. Phys. Chem. B*, 2002, **106**, 3538–3542.
170 M. J. Giz, B. Duong and N. J. Tao, *J. Electroanal. Chem.*, 1999, **465**, 72–79.
171 M. S. Yeganeh, S. M. Dougal, R. S. Polizzotti and P. Rabinowitz, *Phys. Rev. Lett.*, 1995, **74**, 1811–1814.
172 F. Terán Arce, M. E. Vela, R. C. Salvarezza and A. J. Arvia, *J. Chem. Phys.*, 1998, **109**, 5703–5706.
173 X. Torrelles, E. Barrena, C. Munuera, J. Rius, S. Ferrer and C. Ocal, *Langmuir*, 2004, **20**, 9396–9402.
174 K. Kobayashi, H. Yamada, T. Horiuchi and K. Matsushige, *Jpn. J. Appl. Phys.*, 1998, **37**(part 1), 6183–6185.
175 E. Barrena, E. Palacios-Lidón, C. Munuera, X. Torrelles, S. Ferrer, U. Jonas, M. Salmeron and C. Ocal, *J. Am. Chem. Soc.*, 2004, **126**, 385–395.
176 H. Hagenstrom, M. A. Schneeweiss and D. M. Kolb, *Langmuir*, 1999, **15**, 2435–2443.
177 G. Benitez, C. Vericat, S. Tanco, F. Remes Lenicov, M. F. Castez, M. E. Vela and R. C. Salvarezza, *Langmuir*, 2004, **20**, 5030–5037.
178 C. A. Widrig, C. A. Alves and M. D. Porter, *J. Am. Chem. Soc.*, 1991, **113**, 2805–2810.
179 O. Voznyy, J. J. Dubowski, J. T. Yates and P. Maksymovych, *J. Am. Chem. Soc.*, 2009, **131**, 12989–12993.
180 H. Kondoh and H. Nozoye, *J. Phys. Chem. B*, 1999, **103**, 2585–2588.
181 V. De Renzi, R. Di Felice, D. Marchetto, R. Biagi, U. del Pennino and A. Selloni, *J. Phys. Chem. B*, 2004, **108**, 16–20.
182 T. Sawaguchi, F. Mizutani and I. Taniguchi, *Langmuir*, 1998, **14**, 3565–3569.
183 L.-J. Wan, Y. Hara, H. Noda and M. Osawa, *J. Phys. Chem. B*, 1998, **102**, 5943–5946.
184 Zhou, T. Baunach, V. Ivanova and D. M. Kolb, *Langmuir*, 2004, **20**, 4590–4595.
185 W. Andreoni, A. Curioni and H. Grönbeck, *Int. J. Quantum Chem.*, 2000, **80**, 598–608.
186 K. M. Beardmore, J. D. Kress, N. Grönbech-Jensen and A. R. Bishop, *Chem. Phys. Lett.*, 1998, **286**, 40–45.
187 K. M. Beardmore, J. D. Kress, A. R. Bishop and N. Grönbech-Jensen, *Synth. Met.*, 1997, **84**, 317–318.
188 H. Grönbeck, A. Curioni and W. Andreoni, *J. Am. Chem. Soc.*, 2000, **122**, 3839–3842.
189 Y. Yourdshahyan, H. K. Zhang and A. M. Rappe, *Phys. Rev. B*, 2001, **63**, 081405.
190 M. C. Vargas, P. Giannozzi, A. Selloni and G. Scoles, *J. Phys. Chem. B*, 2001, **105**, 9509–9513.
191 T. Hayashi, Y. Morikawa and H. Nozoye, *J. Chem. Phys.*, 2001, **114**, 7615–7621.
192 Y. Akinaga, T. Nakajima and K. Hirao, *J. Chem. Phys.*, 2001, **114**, 8555–8564.
193 J. Gottschalck and B. Hammer, *J. Chem. Phys.*, 2002, **116**, 784–790.
194 Y. Yourdshahyan and A. M. Rappe, *J. Chem. Phys.*, 2002, **117**, 825–833.
195 S. Franzen, *Chem. Phys. Lett.*, 2003, **381**, 315–321.
196 F. P. Cometto, P. Paredes-Olivera, V. A. Macagno and E. M. Patrito, *J. Phys. Chem. B*, 2005, **109**, 21737–21748.
197 M. Tachibana, K. Yoshizawa, A. Ogawa, H. Fujimoto and R. Hoffmann, *J. Phys. Chem. B*, 2002, **106**, 12727–12736.
198 H. Kondoh, M. Iwasaki, T. Shimada, K. Amemiya, T. Yokoyama, T. Ohta, M. Shimomura and S. Kono, *Phys. Rev. Lett.*, 2003, **90**, 066102.
199 M. G. Roper, M. P. Skegg, C. J. Fisher, J. J. Lee, V. R. Dhanak, D. P. Woodruff and R. G. Jones, *Chem. Phys. Lett.*, 2004, **389**, 87–91.
200 L. M. Molina and B. Hammer, *Chem. Phys. Lett.*, 2002, **360**, 264–271.
201 Y. Morikawa, C. Liew and H. Nozoye, *Surf. Sci.*, 2002, **514**, 389–393.
202 M. Yu, N. Bovet, C. J. Satterley, S. Bengió, K. R. J. Lovelock, P. K. Milligan, R. G. Jones, D. P. Woodruff and V. Dhanak, *Phys. Rev. Lett.*, 2006, **97**, 166102.
203 A. Chaudhuri, T. J. Lerotholi, D. C. Jackson, D. P. Woodruff and V. Dhanak, *Phys. Rev. Lett.*, 2009, **102**, 126101.
204 R. Mazzarello, A. Cossaro, A. Verdini, R. Rousseau, L. Casalis, M. F. Danisman, L. Floreano, S. Scandolo, A. Morgante and G. Scoles, *Phys. Rev. Lett.*, 2007, **98**, 016102.
205 A. Cossaro, R. Mazzarello, R. Rousseau, L. Casalis, A. Verdini, A. Kohlmeyer, L. Floreano, S. Scandolo, A. Morgante, M. L. Klein and G. Scoles, *Science*, 2008, **321**, 943–946.
206 H. Gronbeck and H. Hakkinen, *J. Phys. Chem. B*, 2007, **111**, 3325–3327.
207 H. Hakkinen, M. Walter and H. Gronbeck, *J. Phys. Chem. B*, 2006, **110**, 9927–9931.
208 D.-e. Jiang and S. Dai, *J. Phys. Chem. C*, 2009, **113**, 7838–7842.
209 H. Grönbeck, H. Häkkinen and R. L. Whetten, *J. Phys. Chem. C*, 2008, **112**, 15940–15942.
210 D.-e. Jiang, *Chem. Phys. Lett.*, 2009, **477**, 90–94.
211 O. Voznyy and J. J. Dubowski, *Langmuir*, 2009, **25**, 7353–7358.
212 P. Maksymovych and J. T. Yates, *J. Am. Chem. Soc.*, 2008, **130**, 7518–7519.
213 D. C. Jackson, A. Chaudhuri, T. J. Lerotholi, D. P. Woodruff, R. G. Jones and V. R. Dhanak, *Surf. Sci.*, 2009, **603**, 807–813.
214 P. D. Jadzinsky, G. Calero, C. J. Ackerson, D. A. Bushnell and R. D. Kornberg, *Science*, 2007, **318**, 430–433.
215 K. Reuter and M. Scheffler, *Phys. Rev. B*, 2002, **65**, 165403.
216 P. Carro, R. Salvarezza, D. Torres and F. Illas, *J. Phys. Chem. C*, 2008, **112**, 19121–19124.
217 I. Touzov and C. B. Gorman, *J. Phys. Chem. B*, 1997, **101**, 5263–5276.
218 F. Terán Arce, M. E. Vela, R. C. Salvarezza and A. J. Arvia, *Langmuir*, 1998, **14**, 7203–7212.
219 C. Vericat, G. Andreasen, M. E. Vela, H. Martin and R. C. Salvarezza, *J. Chem. Phys.*, 2001, **115**, 6672–6678.
220 C. E. Bach, M. Giesen, H. Ibach and T. L. Einstein, *Phys. Rev. Lett.*, 1997, **78**, 4225–4228.
221 N. A. Kautz and S. A. Kandel, *J. Am. Chem. Soc.*, 2008, **130**, 6908–6909.
222 D. Hobara, M. Yamamoto and T. Kakiuchi, *Chem. Lett.*, 2001, 374–375.
223 M. J. Esplandiu, M. L. Carot, F. P. Cometto, V. A. Macagno and E. M. Patrito, *Surf. Sci.*, 2006, **600**, 155–172.
224 H. Wano and K. Uosaki, *Langmuir*, 2005, **21**, 4024–4033.
225 D. F. Yang, C. P. Wilde and M. Morin, *Langmuir*, 1996, **12**, 6570–6577.
226 M. E. Vela, H. Martin, C. Vericat, G. Andreasen, A. Hernández Creus and R. C. Salvarezza, *J. Phys. Chem. B*, 2000, **104**, 11878–11882.
227 T. Kawaguchi, H. Yasuda, K. Shimazu and M. D. Porter, *Langmuir*, 2000, **16**, 9830–9840.
228 M. Yu, N. Bovet, C. J. Satterley, S. Bengio, K. R. J. Lovelock, P. K. Milligan, R. G. Jones, D. P. Woodruff and V. Dhanak, *Phys. Rev. Lett.*, 2006, **97**, 166102.
229 D. Hobara, K. Miyake, S.-I. Imabayashi, K. Niki and T. Kakiuchi, *Langmuir*, 1998, **14**, 3590–3596.
230 L. Xi, Z. Zheng, N.-S. Lam, H.-Y. Nie, O. Grizzi and W.-M. Lau, *J. Phys. Chem. C*, 2008, **112**, 12111–12115.
231 G. Yang and G.-y. Liu, *J. Phys. Chem. B*, 2003, **107**, 8746–8759.
232 C. Fuxen, W. Azzam, R. Arnold, G. Witte, A. Terfort and C. Wöll, *Langmuir*, 2001, **17**, 3689–3695.
233 C. Schoenenberger, J. Jorritsma, J. A. M. Sondag-Huethorst and L. G. J. Fokkink, *J. Phys. Chem.*, 1995, **99**, 3259–3271.
234 J.-P. Bucher, L. Santesson and K. Kern, *Langmuir*, 1994, **10**, 979–983.
235 J. A. M. Sondag-Huethorst, C. Schonenberger and L. G. J. Fokkink, *J. Phys. Chem.*, 1994, **98**, 6826–6834.
236 A. Badia, R. B. Lennox and L. Reven, *Acc. Chem. Res.*, 2000, **33**, 475–481.

237 M. J. Capitán, J. Álvarez, J. J. Calvente and R. Andreu, *Angew. Chem., Int. Ed.*, 2006, **45**, 6166–6169.
238 M. D. Porter, T. B. Bright, D. L. Allara and C. E. D. Chidsey, *J. Am. Chem. Soc.*, 1987, **109**, 3559–3568.
239 N. Camillone III, C. E. D. Chidsey, G.-Y. Liu, T. M. Putvinski and G. Scoles, *J. Chem. Phys.*, 1991, **94**, 8493–8502.
240 A. Badia, S. Singh, L. Demers, L. Cuccia, G. R. Brown and R. B. Lennox, *Chem.–Eur. J.*, 1996, **2**, 359–363.
241 C. H. Kagan, *NSF-CONICET Quilmes Nanoscience Workshop: Electronic with Molecules and Quantum Dots*, Ruinas de Quilmes, Argentina, 2003.
242 H. Schmitt, A. Badia, L. Dickinson, L. Reven, R. Lennox and n. Bruce, *Adv. Mater.*, 1998, **10**, 475.
243 W. Gao and L. Reven, *Langmuir*, 1995, **11**, 1860–1863.
244 S. Subramanian and S. Sampath, *Anal. Bioanal. Chem.*, 2007, **388**, 135–145.
245 P. Kohli, K. K. Taylor, J. J. Harris and G. J. Blanchard, *J. Am. Chem. Soc.*, 1998, **120**, 11962–11968.
246 M. J. Esplandiu, H. Hagenstrom and D. M. Kolb, *Langmuir*, 2001, **17**, 828–838.
247 M. L. Carot, M. J. Esplandiu, F. P. Cometto, E. M. Patrito and V. A. Macagno, *J. Electroanal. Chem.*, 2005, **579**, 13–23.
248 E. Delamarche, B. Michel, C. Gerber, D. Anselmetti, H. J. Guentherodt, H. Wolf and H. Ringsdorf, *Langmuir*, 1994, **10**, 2869–2871.
249 L. A. Bumm, J. J. Arnold, L. F. Charles, T. D. Dunbar, D. L. Allara and P. S. Weiss, *J. Am. Chem. Soc.*, 1999, **121**, 8017–8021.
250 C. M. A. Brett, K. Slavoj, H. Tibor and A. M. Oliveira Brett, *Electroanalysis*, 2003, **15**, 557–565.
251 M. Kind and C. Wöll, *Prog. Surf. Sci.*, 2009, **84**, 230–278.
252 T. Baunach, V. Ivanova, D. M. Kolb, H. G. Boyen, P. Ziemann, M. Büttner and P. Oelhafen, *Adv. Mater.*, 2004, **16**, 2024–2028.
253 Y. Tai, A. Shaporenko, H. Noda, M. Grunze and M. Zharnikov, *Adv. Mater.*, 2005, **17**, 1745–1749.
254 K. Rajalingam, T. Strunskus, A. Terfort, R. A. Fischer and C. Wöll, *Langmuir*, 2008, **24**, 7986–7994.
255 J. Weiss, H.-J. Himmel, R. A. Fischer and C. Wöll, *Adv. Mater.*, 1998, **10**, 17–21.
256 D. M. Adams, L. Brus, C. E. D. Chidsey, S. Creager, C. Creutz, C. R. Kagan, P. V. Kamat, M. Lieberman, S. Lindsay, R. A. Marcus, R. M. Metzger, M. E. Michel-Beyerle, J. R. Miller, M. D. Newton, D. R. Rolison, O. Sankey, K. S. Schanze, J. Yardley and X. Zhu, *J. Phys. Chem. B*, 2003, **107**, 6668–6697.
257 C. Vericat, F. Remes Lenicov, S. Tanco, G. Andreasen, M. E. Vela and R. C. Salvarezza, *J. Phys. Chem. B*, 2002, **106**, 9114–9121.
258 W. Knoll, I. Köper, R. Naumann and E. K. Sinner, *Electrochim. Acta*, 2008, **53**, 6680–6689.
259 P. E. Sheehan and L. J. Whitman, *Phys. Rev. Lett.*, 2002, **88**, 156104.
260 J. A. Helmuth, H. Schmid, R. Stutz, A. Stemmer and H. Wolf, *J. Am. Chem. Soc.*, 2006, **128**, 9296–9297.
261 J. M. McLellan, M. Geissler and Y. Xia, *J. Am. Chem. Soc.*, 2004, **126**, 10830–10831.
262 A. A. Dameron, J. R. Hampton, R. K. Smith, T. J. Mullen, S. D. Gillmor and P. S. Weiss, *Nano Lett.*, 2005, **5**, 1834–1837.
263 L. A. Adamczyk and M. R. Anderson, *J. Colloid Interface Sci.*, 2009, **336**, 761–765.
264 N. G. Tognalli, A. Fainstein, C. Vericat, M. E. Vela and R. C. Salvarezza, *J. Phys. Chem. B*, 2006, **110**, 354–360.
265 N. G. Tognalli, A. Fainstein, C. Vericat, M. E. Vela and R. C. Salvarezza, *J. Phys. Chem. C*, 2008, **112**, 3741–3746.
266 D. Grumelli, C. Vericat, G. Benitez, M. E. Vela, R. C. Salvarezza, L. J. Giovanetti, J. M. Ramallo-López, F. G. Requejo, A. F. Craievich and Y. S. Shon, *J. Phys. Chem. C*, 2007, **111**, 7179–7184.
267 C. J. Zhong, R. C. Brush, J. Anderegg and M. D. Porter, *Langmuir*, 1999, **15**, 518–525.
268 Y. W. Yang and L. J. Fan, *Langmuir*, 2002, **18**, 1157–1164.
269 D. G. Castner, K. Hinds and D. W. Grainger, *Langmuir*, 1996, **12**, 5083–5086.
270 C. Vericat, G. A. Benitez, D. E. Grumelli, M. E. Vela and R. C. Salvarezza, *J. Phys.: Condens. Matter*, 2008, **20**, 184004.
271 M. H. Schoenfisch and J. E. Pemberton, *J. Am. Chem. Soc.*, 1998, **120**, 4502–5413.
272 A. C. Templeton, W. P. Wuelfing and R. W. Murray, *Acc. Chem. Res.*, 2000, **33**, 27–36.
273 C. Gutiérrez-Wing, J. A. Ascencio, M. Pérez-Alvarez, M. Marín-Almazo and M. José-Yacamán, *J. Cluster Sci.*, 1998, **9**, 529–545.
274 W. D. Luedtke and U. Landman, *J. Phys. Chem.*, 1996, **100**, 13323–13329.
275 W. D. Luedtke and U. Landman, *J. Phys. Chem. B*, 1998, **102**, 6566–6572.
276 J. M. Ramallo-Lopez, L. J. Giovanetti, F. G. Requejo, S. R. Isaacs, Y. S. Shon and M. Salmeron, *Phys. Rev. B*, 2006, **74**, 073410.
277 T. Pradeep and N. Sandhyarani, *Pure Appl. Chem.*, 2002, **741**, 593–1607.
278 A. C. Templeton, M. J. Hostetler, E. K. Warmoth, S. Chen, C. M. Hartshorn, V. M. Krishnamurthy, M. D. E. Forbes and R. W. Murray, *J. Am. Chem. Soc.*, 1998, **120**, 4845–4849.
279 A. Badia, L. Cuccia, L. Demers, F. Morin and R. B. Lennox, *J. Am. Chem. Soc.*, 1997, **119**, 2682.
280 M. J. Hostetler, J. J. Stokes and R. W. Murray, *Langmuir*, 1996, **12**, 3604.
281 K. Heister, M. Zharnikov, M. Grunze and L. S. O. Johansson, *J. Phys. Chem. B*, 2001, **105**, 4058–4061.
282 M. C. Bourg, A. Badia and R. Bruce Lennox, *J. Phys. Chem. B*, 2000, **104**, 6562–6567.
283 P. G. Lustemberg, C. Vericat, G. A. Benitez, M. E. Vela, N. Tognalli, A. Fainstein, M. L. Martiarena and R. C. Salvarezza, *J. Phys. Chem. C*, 2008, **112**, 11394–11402.
284 R. F. W. Bader, *Atoms in Molecules–A, Quantum Theory*, Oxford University Press, Oxford, UK, 1990.
285 W. Tang, E. Sanville and G. Henkelman, *J. Phys.: Condens. Matter*, 2009, **21**, 084204.
286 B. de Boer, A. Hadipour, M. M. Mandoc, T. van Woudenbergh and P. W. M. Blom, *Adv. Mater.*, 2005, **17**, 621–625.
287 V. De Renzi, R. Rousseau, D. Marchetto, R. Biagi, S. Scandolo and U. del Pennino, *Phys. Rev. Lett.*, 2005, **95**, 046804.
288 P. C. Rusu and G. Brocks, *J. Phys. Chem. B*, 2006, **110**, 22628–22634.
289 P. C. Rusu and G. Brocks, *Phys. Rev. B*, 2006, **74**, 073414.
290 P. Zhang and T. K. Sham, *Phys. Rev. Lett.*, 2003, **90**, 245502.
291 P. Moriarty, *Phys. Rev. Lett.*, 2004, **92**, 109601.
292 A. Tanaka, Y. Takeda, M. Imamura and S. Sato, *Phys. Rev. B*, 2003, **68**, 195415.
293 A. Tanaka, Y. Takeda, T. Nagasawa and K. Takahashi, *Solid State Commun.*, 2003, **126**, 191–196.
294 Y. Kitsudo, A. Iwamoto, H. Matsumoto, K. Mitsuhara, T. Nishimura, M. Takizawa, T. Akita, Y. Maeda and Y. Kido, *Surf. Sci.*, 2009, **603**, 2108–2114.
295 M. Büttner, H. Kröger, I. Gerhards, D. Mathys and P. Oelhafen, *Thin Solid Films*, 2006, **495**, 180–185.
296 P. Crespo, R. Litrán, T. C. Rojas, M. Multigner, J. M. de la Fuente, J. C. Sánchez-López, M. A. García, A. Hernando, S. Penadés and A. Fernández, *Phys. Rev. Lett.*, 2004, **93**, 087204.
297 R. Berger, E. Delamarche, H. P. Lang, C. Gerber, J. K. Gimzewski, E. Meyer and H.-J. Guntherodt, *Science*, 1997, **276**, 2021–2024.
298 H. Hori, T. Teranishi, Y. Nakae, Y. Seino, M. Miyake and S. Yamada, *Phys. Lett. A*, 1999, **263**, 406–410.
299 X. Huang, P. K. Jain, I. H. El-Sayed and M. A. El-Sayed, *Nanomedicine*, 2007, **2**, 681–693.
300 Y. Negishi, H. Tsunoyama, M. Suzuki, N. Kawamura, M. M. Matsushita, K. Maruyama, T. Sugawara, T. Yokoyama and T. Tsukuda, *J. Am. Chem. Soc.*, 2006, **128**, 12034–12035.
301 J. S. Garitaonandia, M. Insausti, E. Goikolea, M. Suzuki, J. D. Cashion, N. Kawamura, H. Ohsawa, I. Gil de Muro, K. Suzuki, F. Plazaola and T. Rojo, *Nano Lett.*, 2008, **8**, 661–667.
302 P. Dutta, S. Pal, M. S. Seehra, M. Anand and C. B. Roberts, *Appl. Phys. Lett.*, 2007, **90**, 213102–213103.
303 E. Goikolea, J. S. Garitaonandia, M. Insausti, J. Lago, I. Gil de Muro, J. Salado, F. J. Bermejo and D. Schmool, *J. Non-Cryst. Solids*, 2008, **354**, 5210–5212.
304 Z. Vager, I. Carmeli, G. Leitus, S. Reich and R. Naaman, *J. Phys. Chem. Solids*, 2004, **65**, 713–717.

305 I. Carmeli, G. Leitus, R. Naaman, S. Reich and Z. Vager, *J. Chem. Phys.*, 2003, **118**, 10372–10375.
306 S. G. Ray, S. S. Daube, G. Leitus, Z. Vager and R. Naaman, *Phys. Rev. Lett.*, 2006, **96**, 036101.
307 E. Guerrero, M. A. Munoz-Marquez, M. A. Garcia, P. Crespo, E. Fernandez-Pinel, A. Hernando and A. Fernandez, *Nanotechnology*, 2008, **19**, 175701.
308 J. De la Venta, E. Fernández Pinel, M. A. García, P. Crespo, A. Hernando, O. Rodríguez de la Fuento, C. de Julián Fernández, A. Fernández and S. Penadés, *Mod. Phys. Lett. B*, 2007, **21**, 303–319.
309 A. Hernando, P. Crespo and M. A. Garcia, *Phys. Rev. Lett.*, 2006, **96**, 057206.
310 P. de la Presa, M. Multigner, J. de la Venta, M. A. Garcia and M. L. Ruiz-Gonzalez, *J. Appl. Phys.*, 2006, **100**, 123915–123916.
311 M. Suda, N. Kameyama, A. Ikegami, M. Suzuki, N. Kawamura and Y. Einaga, *Polyhedron*, 2009, **28**, 1868–1874.
312 F. Michael, C. Gonzalez, V. Mujica, M. Marquez and M. A. Ratner, *Phys. Rev. B*, 2007, **76**, 224409.
313 A. Hernando, P. Crespo, M. A. Garcia, E. F. Pinel, J. de la Venta, A. Fernandez and S. Penades, *Phys. Rev. B*, 2006, **74**, 052403.
314 A. M. Moulin, S. J. O'Shea and M. E. Welland, *Ultramicroscopy*, 2000, **82**, 23–31.
315 V. Tabard-Cossa, M. Godin, I. J. Burgess, T. Monga, R. B. Lennox and P. Grutter, *Anal. Chem.*, 2007, **79**, 8136–8143.
316 R. Desikan, I. Lee and T. Thundat, *Ultramicroscopy*, 2006, **106**, 795–799.
317 J. Fritz, M. K. Baller, H. P. Lang, T. Strunz, E. Meyer, H. J. Guntherodt, E. Delamarche, C. Gerber and J. K. Gimzewski, *Langmuir*, 2000, **16**, 9694–9696.
318 M. H. Dishner, J. C. Hemminger and F. J. Feher, *Langmuir*, 1997, **13**, 2318–2322.
319 M. Godin, *PhD Thesis*, McGill University, 2004.
320 M. Godin, V. Tabard-Cossa, P. Grutter and P. Williams, *Appl. Phys. Lett.*, 2001, **79**, 551–553.
321 X. Yi and H. L. Duan, *J. Mech. Phys. Solids*, 2009, **57**, 1254–1266.
322 R. L. McCreery, *Chem. Mater.*, 2004, **16**, 4477–4496.
323 A. Salomon, D. Cahen, S. Lindsay, J. Tomfohr, V. B. Engelkes and C. D. Frisbie, *Adv. Mater.*, 2003, **15**, 1881–1890.
324 S. Datta, W. Tian, S. Hong, R. Reifenberger, J. I. Henderson and C. P. Kubiak, *Phys. Rev. Lett.*, 1997, **79**, 2530–2533.
325 A. P. Labonte, S. L. Tripp, R. Reifenberger and A. Wei, *J. Phys. Chem. B*, 2002, **106**, 8721–8725.
326 X. D. Cui, A. Primak, X. Zarate, J. Tomfohr, O. F. Sankey, A. L. Moore, T. A. Moore, D. Gust, G. Harris and S. M. Lindsay, *Science*, 2001, **294**, 571–574.
327 D. J. Wold and C. D. Frisbie, *J. Am. Chem. Soc.*, 2001, **123**, 5549–5556.
328 J. R. Heath and M. A. Ratner, *Phys. Today*, 2003, **56**, 43.
329 C. Joachim, J. K. Gimzewski and A. Aviram, *Nature*, 2000, **408**, 541–548.
330 J. Kushmerick, S. K. Pollack, J. C. Yang, J. Naciri, D. B. Holt, M. A. Ratner and R. Shashidhar, *Ann. N. Y. Acad. Sci.*, 2003, **1006**, 277–290.
331 Y. A. Ovchenkov, H. Geisler, J. M. Burst, S. N. Thornburg, C. A. Ventrice, C. Zhang, J. Redepenning, Y. Losovyj, L. Rosa, P. A. Dowben and B. Doudin, *Chem. Phys. Lett.*, 2003, **381**, 7–13.
332 X. Xiao, B. Xu and N. J. Tao, *Nano Lett.*, 2004, **4**, 267–271.
333 X. Li, J. He, J. Hihath, B. Xu, S. M. Lindsay and N. Tao, *J. Am. Chem. Soc.*, 2006, **128**, 2135–2141.
334 J. He and S. M. Lindsay, *J. Am. Chem. Soc.*, 2005, **127**, 11932–11933.
335 I. Visoly-Fisher, K. Daie, Y. Terazono, C. Herrero, F. Fungo, L. Otero, E. Durantini, J. J. Silber, L. Sereno, D. Gust, T. A. Moore, A. L. Moore and S. M. Lindsay, *Proc. Natl. Acad. Sci. U. S. A.*, 2006, **103**, 8686–8690.
336 L. Patrone, S. Palacin, J. Charlier, F. Armand, J. P. Bourgoin, H. Tang and S. Gauthier, *Phys. Rev. Lett.*, 2003, **91**, 096802.
337 J. M. Beebe, V. B. Engelkes, L. L. Miller and C. D. Frisbie, *J. Am. Chem. Soc.*, 2002, **124**, 11268–11269.
338 F. Chen, X. Li, J. Hihath, Z. Huang and N. Tao, *J. Am. Chem. Soc.*, 2006, **128**, 15874–15881.
339 J. Ulrich, D. Esrail, W. Pontius, L. Venkataraman, D. Millar and L. H. Doerrer, *J. Phys. Chem. B*, 2006, **110**, 2462–2466.
340 A. M. Ricci, E. J. Calvo, S. Martin and R. J. Nichols, *J. Am. Chem. Soc.*, 2010, **132**(8), 2494–2495.
341 N. D. Lang and C. R. Kagan, *Nano Lett.*, 2006, **6**, 2955–2958.
342 Y. Xue, S. Datta and M. A. Ratner, *J. Chem. Phys.*, 2001, **115**, 4292–4299.
343 G. Heimel, L. Romaner, J.-L. Bredas and E. Zojer, *Phys. Rev. Lett.*, 2006, **96**, 196806.
344 G. Yang, N. A. Amro, Z. B. Starkewolfe and G.-y. Liu, *Langmuir*, 2004, **20**, 3995–4003.
345 K. Jans, K. Bonroy, R. De Palma, G. Reekmans, H. Jans, W. Laureyn, M. Smet, G. Borghs and G. Maes, *Langmuir*, 2008, **24**, 3949–3954.
346 T. M. Willey, A. L. Vance, T. van Buuren, C. Bostedt, L. J. Terminello and C. S. Fadley, *Surf. Sci.*, 2005, **576**, 188–196.
347 M. Lewis, M. Tarlov and K. Carron, *J. Am. Chem. Soc.*, 1995, **117**, 9574–9575.
348 Y. Zhang, R. H. Terrill and P. W. Bohn, *Chem. Mater.*, 1999, **11**, 2191–2198.
349 N. Garg, E. Carrasquillo-Molina and T. R. Lee, *Langmuir*, 2002, **18**, 2717–2726.
350 E. Ito, J. Noh and M. Hara, *Chem. Phys. Lett.*, 2008, **462**, 209–212.
351 D. A. Hutt and G. J. Leggett, *J. Phys. Chem.*, 1996, **100**, 6657–6662.
352 M. T. Lee, C. C. Hsueh, M. S. Freund and G. S. Ferguson, *Langmuir*, 1998, **14**, 6419–6423.
353 N. T. Flynn, T. N. T. Tran, M. J. Cima and R. Langer, *Langmuir*, 2003, **19**, 10909–10915.
354 H. Kondoh, C. Kodama and H. Nozoye, *J. Phys. Chem. B*, 1998, **102**, 2310–2312.
355 H. Kondoh, C. Kodama, H. Sumida and H. Nozoye, *J. Chem. Phys.*, 1999, **111**, 1175–1184.
356 J. B. Schlenoff, M. Li and H. Ly, *J. Am. Chem. Soc.*, 1995, **117**, 12528–12536.
357 R. G. Nuzzo, B. R. Zegarski and L. H. Dubois, *J. Am. Chem. Soc.*, 1987, **109**, 733–740.
358 C. Vericat, G. A. Benitez, D. E. Grumelli, M. E. Vela and R. C. Salvarezza, *J. Phys.: Condens. Matter*, 2008, **20**, 184004.
359 J. Noh, H. S. Kato, M. Kawai and M. Hara, *J. Phys. Chem. B*, 2006, **110**, 2793.
360 B. D. Lamp, D. Hobara, M. D. Porter, K. Niki and T. M. Cotton, *Langmuir*, 1997, **13**, 736–741.
361 E. Cortés, A. A. Rubert, G. Benitez, P. Carro, M. E. Vela and R. C. Salvarezza, *Langmuir*, 2009, **25**, 5661–5666.
362 N. G. Tognalli, A. Fainstein, C. Vericat, M. E. Vela and R. C. Salvarezza, *J. Phys. Chem. C*, 2008, **112**, 3741–3746.
363 C. Vericat, G. A. Benitez, M. E. Vela, R. C. Salvarezza, N. G. Tognalli and A. Fainstein, *Langmuir*, 2007, **23**, 1152–1159.
364 Y. Chen, R. E. Palmer and J. P. Wilcoxon, *Langmuir*, 2006, **22**, 2851–2855.
365 R. Ristau, R. Tiruvalam, P. L. Clasen, E. P. Gorskowski, M. P. Harmer, C. J. Kiely, I. Hussain and M. Brust, *Gold Bull.*, 2009, **42**, 133–143.
366 R. Balasubramanian, Y.-G. Kwon and A. Wei, *J. Mater. Chem.*, 2007, **17**, 105–112.
367 N. Nishida, M. Hara, H. Sasabe and W. Knoll, *Jpn. J. Appl. Phys.*, 1996, **35**(part 1), 5866–5872.
368 D. J. Lavrich, S. M. Wetterer, S. L. Bernasek and G. Scoles, *J. Phys. Chem. B*, 1998, **102**, 3456–3465.
369 R. Staub, M. Toerker, T. Fritz, T. Schmitz-Hübsch, F. Sellam and K. Leo, *Langmuir*, 1998, **14**, 6693–6698.
370 C. Kodama, T. Hayashi and H. Nozoye, *Appl. Surf. Sci.*, 2001, **169–170**, 264–267.
371 N. Nishida, M. Hara, H. Sasabe and W. Knoll, *Jpn. J. Appl. Phys.*, 1996, **35**(part 2), L799–L802.
372 M. Buttner, *PhD Thesis*, Basel University, 2006.
373 G. K. Jennings and P. E. Laibinis, *Langmuir*, 1996, **12**, 6173–6175.
374 R. Valiokas, M. Ostblom, S. Svedhem, S. C. T. Svensson and B. Liedberg, *J. Phys. Chem. B*, 2002, **106**, 10401–10409.
375 A. Turchanin, D. Kafer, M. El-Desawy, C. Wöll, G. Witte and A. Golzhauser, *Langmuir*, 2009, **25**, 7342–7352.

